

One-dimensional extended Hubbard model in the atomic limit

F. Mancini

*Dipartimento di Fisica E. R. Caianiello - Unità CNISM di Salerno
Università degli Studi di Salerno, Via S. Allende, I-84081 Baronissi (SA), Italy*

F. P. Mancini

*Dipartimento di Fisica and Sezione I.N.F.N.
Università degli Studi di Perugia,
Via A. Pascoli, I-06123 Perugia, Italy*

(Dated: July 25, 2008)

We present the exact solution of the one-dimensional extended Hubbard model in the atomic limit within the Green's function and equation of motion formalism. We provide a comprehensive and systematic analysis of the model by considering all the relevant response and correlation functions as well as thermodynamic quantities in the whole parameter space. At zero temperature we identify four phases in the plane (U, n) (U is the on-site potential and n is the filling) and relative phase transitions as well as different types of charge ordering. These features are endorsed by investigating at $T = 0$ the chemical potential and pertinent local correlators, the particle and double occupancy correlation functions, the entropy, and by studying the behavior in the limit $T \rightarrow 0$ of the charge and spin susceptibilities. A detailed study of the thermodynamic quantities is also presented at finite temperature. This study evidences that a finite-range order persists for a wide range of the temperature, as shown by the behavior of the correlation functions and by the two-peak structure exhibited by the charge susceptibility and by the entropy. Moreover, the equation of motion formalism, together with the use of composite operators, allows us to exactly determine the set of elementary excitations. As a result, the density of states can be determined exactly and a detailed analysis of the specific heat allows for identifying the excitations and for ascribing its two-peak structure to a redistribution of the charge density.

I. INTRODUCTION

It goes without saying that the Hubbard model [1] is of seminal importance in the study of modern condensed matter theory. Originally introduced to describe the correlations of electrons in the narrow d band of transition metals, the Hubbard model has been subsequently used to investigate a large variety of situations experimentally observed. Upon varying the model parameters, it is believed that the Hubbard model can describe many properties of strongly correlated electronic systems. However, its applicability to real materials is rather limited and some extensions are needed. Among various generalizations, one of the most studied is the so-called extended Hubbard model (EHM), where a nearest-neighbor interaction V is added to the original Hubbard Hamiltonian, which includes only an on-site interaction U . If one assumes that the interaction parameters arise solely from Coulomb interactions, then both U and V are repulsive. However, these parameters may represent effective interactions. Thus their ranges can be broader, allowing for both positive and negative values. The electronic properties of the model are substantially modified by including nonlocal interactions allowing one to study general features of doped systems like copper-oxide materials [2], high-temperature superconductors [3], manganese compounds [4], and to describe charge ordering (CO), experimentally observed, in a variety of systems. Indeed, several studies of the extended Hubbard model have pointed to the presence of states with phase separation [5] and of

charge-ordered phases [6, 7]. Furthermore, the introduction of an intersite interaction can mime longer-ranged Coulomb interactions needed to describe effects observed in conducting polymers [8].

Although the Hubbard model is oversimplified and in spite of very intensive study, both analytical and numerical, exact solutions exist only in one or infinite dimensions. In 1D the thermodynamics of the Hubbard model has been widely investigated by means of different exact approaches for both nearest-neighbor hopping [9, 10] and long-range hopping [11]. For higher dimensions ($D > 1$), the study is far from being completed and only few rigorous results are known. In particular, relevant results were obtained by exact diagonalization on small clusters [12] and by numerical investigations [13]. For the case of infinite dimension, an exact solution has been obtained by dynamical field theory [14].

The situation is more severe for the extended version of the model: even in 1D there is not a complete exact solution. A particular extended version has been examined in Ref. [15], where a kinetic term (Y) for paired carriers is added to the usual electron hopping (t). The model has been solved only in the particular case of $t = -Y$. Actually, it is known that the EHM is non-integrable for general values of the model parameters [16]. These difficulties have led to the investigation of the so-called narrow band limit, where the hopping t can be neglected with respect to the interaction couplings U and V . This simplified version, also known as the atomic limit of the extended Hubbard model (AL-EHM), has been largely studied for several years.

There is a large and diffused interest in the study of this relatively simple model, motivated by several reasons: (i) the phase diagram has a very rich structure with a multicritical behavior; (ii) one observes several kinds of long-range orders pertinent to commensurate sublattice charge-density alternation (long-range order has been observed in many narrow-band materials, such as $BaBi_xPb_{1-x}O_3$, Cs_2SbCl_6 , Fe_3O_4 , $CsAuCl_3$, and several tetracyanoquinodimethane salts); (iii) the results for the atomic model may give some information beyond the zero-bandwidth limit [several approximate studies, as well as some exact results for the 1D case [17], hint at the possibility that charge ordering persists in the corresponding narrow band model]; (iv) the knowledge of the atomic limit can be used as a starting point for a perturbation expansion in powers of the hopping t .

Without pretending to be exhaustive, a review of the different approaches available in the literature could be presented as follows. The phase diagram of the AL-EHM at half filling ($n = 1$) has been investigated in several papers by means of a modified Hartree-Fock theory [18], beyond Hartree-Fock approximation employing a decoupling procedure [19], variational approach [20] and Bethe-Peierls approximation [21]. The molecular field approximation [22] has been used to obtain the phase diagram in the $(n, U/zV)$ plane and in the $(\mu, U/zV)$ plane (z being the coordination number and μ the chemical potential). Another approach makes use of the transfer-matrix method that, although practically employable only for one-dimensional systems, can provide exact results. In Refs. [23, 24] the specific heat and the static magnetic susceptibility have been studied at half filling. The case of quarter filling, in the limit $U \rightarrow \infty$, has been considered in Ref. [24], where exact expressions for the charge-charge correlation function have been obtained for $n = 1$ and $n = 0.5$ ($U \rightarrow \infty$). For $n = 1$ and $U > 2V$, the ground state is a Mott insulator with one electron per atom; when $U < 2V$ the ground state is a CO state with one sublattice doubly occupied and the other empty. The phase transition (PT) from the CO state to the Mott state can be either first or second order, and the phase diagram exhibits a tricritical point.

A method of constructing the ground state phase diagram has been formulated in Refs. [25] by exploiting the reflection positivity property with respect to reflections in lattice planes exhibited by the AL-EHM. Estimates of the probability of some events at nonzero temperatures were also provided. In Refs. [26] the AL-EHM has been studied in 2D addressing the problem of determining the zero temperature phase diagram in the $(\mu/V, U/V)$ plane. The ground state exhibits several kinds of charge long-range orders, which persist also at sufficiently low temperatures, provided one stays sufficiently far away from the boundary between the different regions. This study reports the absence of PTs among the different regimes at finite temperatures, in contrast to the results of the mean-field approximation [22]. It is also suggested that the staggered charge order persists in the corresponding

narrow band model, although there is no rigorous proof since the reflection positivity property fails to be true for non-zero t .

Another category of studies is based on the use of the Pirogov and Sinai methods [27]. This approach, originally conceived to investigate classical spin systems at low temperatures, has been extended to quantum systems: spin, fermionic and bosonic models. When applied to the AL-EHM, these methods allow for a detailed study of the low temperature phase diagram. Moreover, they allow for an extension to non-zero t , treating the narrow band Hubbard model as a quantum perturbation of the $t = 0$ model. In Ref. [28] the phase diagram of the AL-EHM has been derived. At zero temperature, the phase diagram in the (U, μ) plane shows six phases: three homogeneous (characterized by particle densities $n = 0, 1, 2$ and a staggered charge density $\Delta = 0$) and three staggered (characterized by particle densities $n = 1/2, 1, 3/2$ and staggered charge density $\Delta = 1/2, 1, 1/2$). The staggered order parameter being defined as $\Delta = \lim_{\Lambda \rightarrow \infty} \sum_i \varepsilon(i) n(i) / \Lambda$, where $\varepsilon(i)$ assumes two values, 1 or -1, depending on which sublattice of the bipartite lattice Λ the site i belongs to. For any sufficiently low non-zero temperature, the three staggered phases merge into one, without any PT. These results have been confirmed in Ref. [29], where also the case of attractive intersite potential ($V < 0$) has been considered. The narrow-band extended Hubbard model in $D \geq 2$ has been studied in Ref. [30], where it has been shown that the staggered charge order persists for sufficiently small values of the hopping parameter t . A comprehensive study of the phase diagram of the 1D EHM was carried out in Ref. [31] using different methods: perturbation analysis in the strong and weak coupling limits, quantum Monte Carlo in the intermediate coupling region and exact diagonalization calculations. The authors individuated various phases, including charge and spin density waves, superconductivity, and phase separation. G-ology investigations [32, 33], renormalization group [34], and bosonization [35] studies have provided analytic insights, particularly in the weak coupling regime.

Finally, a large activity by numerical simulation must be mentioned. The EHM has also been studied by means of quantum Monte Carlo (QMC) simulations [36, 37], Lanczos technique [38], exact diagonalization calculations [39, 40], density-matrix renormalization group [41]. The phase diagram and some thermodynamical properties at half filling of the EHM have been studied by means of the density-matrix renormalization group applied to transfer matrices [42]. Recently, some interesting results in the study of the AL-EHM have been obtained by means of Monte Carlo (MC) simulation, for dimensions greater than 1. In Ref. [43], by combining MC and mean-field approximation, the phase diagram at fixed μ has been derived both at $T = 0$ and finite temperatures, and the critical behavior in the vicinity of the tricritical points has been analyzed. In Ref. [44] MC simulation has been used to study the AL-EHM on a square

lattice ($L = 10-40$); a detailed study of the model at finite temperature has been presented for different values of the filling and/or chemical potential, evidencing the presence of different charge orderings and tricritical point lines, and the possibility of phase separation and formation of stripes. The variational cluster approach has also been successfully applied for the EHM in one and two dimensions, showing that QMC and density-matrix renormalization-group results can be reproduced with very good accuracy [45]. Most of these analyses have focused on the half filling case, paying attention to the boundary line separating spin-density wave from charge-density wave, as well as to the existence and location of a tricritical point. In the last few years, there have been discussions galore on the existence of an intermediate bond-order wave phase [46], whose presence seems widely confirmed by now [47]. The case of quarter filling has been examined in several works, providing precise estimates of the charge gap [48], hinting at the possibility of superconductivity in an unexpected region of the (U, V) plane [49] and the existence of a CO transition [6, 40].

As it emerges from the above review, an exact, rigorous and detailed study of the EHM and, in particular, of the one-dimensional case, for different values of the parameters n , T , U , and V , is still missing in the literature. Most of the existing studies have been restricted to the case of half filling. The analysis given in Refs. [26, 28, 29, 30] allows for a complete description of the phase diagram at zero temperature, but in the (μ, U) plane. Moreover, in several works, many properties of the system are presented as a function of the chemical potential μ . Although from a theoretical point of view the chemical potential and the particle density n are conjugated variables, experimentally it is possible to tune the density in a controlled way, by varying the doping. The chemical potential is an internal parameter, dynamically determined by the system itself according to the values of the external parameters. It is very difficult to induce transformations at fixed chemical potential. Moreover, by fixing the particle density or the chemical potential one can obtain different results, if the canonical and grand canonical ensembles are inequivalent due to a divergence of the compressibility. For instance, if the chemical potential is considered as an external parameter, one finds that a solution exists only for discrete values of the particle density ($n = 1/2, 1, 3/2, 2$). Thus, all the studies where μ is considered as an independent variable are doubtless interesting from a mathematical point of view, but are not directly related to experimental situations. It is just more physical to consider the particle density number $n = N_e/N$ - where N_e is the total number of electrons and N is the number of sites - as an external parameter, determined by the particular material under study. In real materials n can vary in a large range: in cuprate materials and in conducting polymers, $n = 1$ (half filling) in the insulating state, but largely varies under doping [8]; in charge transfer salts n varies by varying the pressure in the neighborhood of $n = 2/3$ [50]; Bechgaard salts

have $n = 1/2$ (quarter filling) [51].

It is worthwhile to recall that there is a correspondence between the atomic limit of the extended Hubbard model and the spin-1 Ising model defined on the same lattice. A transformation from the fermionic to the spin Hamiltonian can be performed by defining the pseudospin variable $S(i) = n(i) - 1$. Under this transformation, one ends up with a Hamiltonian pertinent to a spin-1 Ising model with nearest-neighbor exchange $J = -V$, in the presence of an effective crystal field $\Delta = U/2 + k_B T \log 2$ and of an external magnetic field $h = \mu - 2V - U/2$. The temperature dependence of the crystal field is due to the spin degeneracy induced by the mapping between S and n . The literature on the spin-1 Ising model is vast and we refer the interested reader to the bibliography given in Ref. [52]. However, here we would like to comment on the equivalence between the two models. There is a dramatic difference from a physical point of view because, for a spin system, it is possible to tune the magnitude of the applied magnetic field h and vary the temperature T . The system responds to such variations by rearranging the spins in a pertinent configuration, described, in average, by the magnetization $m = \langle S \rangle$. For the fermionic model, the external thermodynamic parameters are n and T : the system responds to variations of these parameters by adjusting the chemical potential μ .

In this work we present a study of the 1D AL-EHM by using a new method based on the equations of motion and Green's function formalism. Recently it has been shown [53] that a system built up of q species of localized Fermi particles subject to finite-range interactions, is exactly solvable in any dimension. By exactly solvable we mean that it is always possible to find a complete set of eigenenergies and eigenoperators of the Hamiltonian closing the hierarchy of the equations of motion. Thus, one can obtain exact expressions for the relevant Green's functions and correlation functions depending on a finite set of parameters, whose knowledge is required in order to have a complete solution of the system. In the case of a one-dimensional lattice, for $q = 1, 2, 3$ [52, 54, 55], and in the case of a Bethe lattice for $q = 1$ [56], it has been shown how it is possible to exactly fix such parameters by means of algebra constraints. The analytical exact solution of the 1D AL-EHM was reported in Ref. [52], where preliminary results were given for vanishing on-site potential. Here we present a systematic and detailed study of the model. We study the properties of the system as a function of the external parameters n , T/V , U/V (throughout the paper we set $V > 0$ as the unit of energy) allowing for the on-site interaction U to be both repulsive and attractive. Owing to the particle-hole symmetry, it is sufficient to explore the interval $[0, 1]$ for the parameter n . The chemical potential is then self-consistently determined as a function of the external parameters. We also address the problem of determining the zero temperature phase diagram in the $(U/V, n)$ plane. Relevant local quantities, such as the double occupancy, the next-nearest correlation functions, the density of states, and

the correlation functions for the charge and double occupancy are systematically computed both at $T = 0$ and as functions of the temperature.

For specific values of the particle density, we find regular spatial distributions of the electrons determined by the two competing terms in the Hamiltonian, i.e., the on-site and the intersite interactions. For particle densities less than quarter filling we do not observe CO states by varying the on-site potential U . At $U = 0$ there is a CO transition at quarter filling from a spatial disordered configuration where the electrons are coupled in pairs to a checkerboard distribution of singly occupied sites for $U > 0$. For particle densities between quarter and half filling, we find three possible spatial arrangements of the electrons by varying U . For attractive on-site potential the electrons are still disorderly coupled in pairs; at $U = 0$ one observes a transition to a peculiar ordered state with alternating empty and occupied sites. The peculiarity consists in the fact that, upon fixing the particle density, some of the singly occupied sites become doubly occupied - with the constraint that the double occupancy D is equal to $(n - 1/2)$ - and the possible distributions along the chain are energetically equivalent. Further increasing the on-site potential, a second transition to a disordered distribution of only singly occupied sites is observed at $U = 2V$. At half filling, we find the well-known transition at $U = 2V$ from a state where every second site is doubly occupied to a state with one electron per site [18]. We also find the interesting result that the correlation functions are controlled by two correlation lengths ξ_n and ξ_D , though the latter is relevant only at $T \neq 0$.

On the other hand, if one fixes the on-site potential and allows the particle density to vary, one observes PTs only at quarter and half filling, signalled by the divergence of the correlation length ξ_n . For fixed attractive on-site potential, the correlation length ξ_n diverges only at half filling and thus, a long-range order is established. For values of on-site potential $0 < U < 2V$ the correlation length ξ_n diverges for all values of the filling in between quarter and half filling, but only at these extremal values does one observe a CO state. For large repulsive on-site potential, ξ_n diverges only at quarter filling, where one finds a regular alternating distribution of singly occupied sites. The further increase of the particle density leads to an increasing single occupation of the empty sites until the homogeneous distribution is reached at half filling.

At finite but low temperatures, one expects that the scenario previously depicted still holds. This wisdom is strengthened by the behavior of thermodynamic quantities such as the compressibility, the charge and spin susceptibilities, the internal energy, the specific heat, and the entropy. The computation of the entropy requires some attention since the ground state is macroscopically degenerate (unless for $U < 2V$ and $n = 1$) and we find, thus, a finite zero-temperature entropy.

Before ending this section, we would like to stress the motivations of our work. Firstly, we use a new method.

The transfer matrix method is the most common approach used in the literature to obtain analytical and exact solutions of the AL-EHM and, thus, allowing for performing explicit calculations of the relevant correlation functions and thermodynamic properties. However, this method is basically restricted to 1D systems. There are great difficulties in extending the method to higher dimensions, as the famous Onsager solution of the 2D spin-1/2 Ising model shows [57]. Our approach has the advantage of offering a general formulation for any dimension [53]. The problem within our approach is that the exact (in principle) solution is expressed in terms of a set of parameters not easily computable by means of the dynamics. The solution of this problem has been found for 1D systems [52, 53, 54, 55] and Bethe lattices [56, 58]; more complicated lattice structures are currently under investigation. Secondly, our approach provides us with an insight into the thermodynamic properties of the AL-EHM. Besides the exact determination of the zero-temperature phase diagram in the full range of the parameters, one is also capable to analyze in detail the behavior of several thermodynamic quantities such as the entropy, the specific heat and the charge and spin susceptibilities. Furthermore, the study of these quantities allows one also to ascertain the different PTs occurring at zero temperature. Last but not least, the Green's function formalism and the equation of motion method allows one to exactly determine the energy spectra and, as a result, to identify the excitation energies contributing to the specific heat. As a consequence, we are able to enlighten the issue of the nature of the peaks in the specific heat: we show that the double-peak structure is only due to charge excitations described by the Hubbard projection operators.

The paper is organized as follows. In Sec. II, upon introducing the Hubbard composite operators, we briefly review the analysis leading to the algebra closure and to analytical expressions of the retarded Green's functions (GF) and correlation functions (CF). Since the composite operators do not satisfy a canonical algebra, the GF and CF depend on a set of internal parameters, leading only to exact relations among the CF. According to the scheme of the composite operator method [59], it is possible to determine these parameters by means of algebra constraints fixing the representation of the GF. By following this scheme, one can obtain extra equations closing the set of relations and allowing for an exact and complete solution of the 1D AL-EHM. In Sec. III we analyze the properties of the system at zero temperature. We characterize the different phases emerging in the phase diagram drawn in the (U, n) plane, by studying the behavior, as functions of n and U , of the chemical potential and of various local properties (double occupancy, next-nearest correlation functions); the density of states and the charge and double occupancy correlation functions are also presented for various values of n and U . In the following, we shall denote with charge and double occupancy, the particle-particle and the dou-

ble occupancy-double occupancy correlation functions, respectively. Section IV is devoted to the study of the finite temperature properties. Further to the study of all the quantities analyzed in Sec. III, we also present results for the compressibility, the charge and spin susceptibilities, the specific heat, and the entropy. Finally, Sec. V is devoted to our conclusions and final remarks, while the appendices report some relevant but rather cumbersome computational details.

II. EXACT SOLUTION OF THE 1D ATOMIC EXTENDED HUBBARD MODEL

The exact solution of the 1D AL-EHM was presented in Ref. [52], where the central issue was the case of vanishing on-site potential ($U = 0$). In this section we shall briefly review the results previously obtained, providing a simpler framework of calculation and extending the solution to nonlocal correlation functions. This new framework allows one to study the properties of the system in the entire region of the external parameters n , T/V , U/V .

By considering the atomic limit, the Hamiltonian of the extended Hubbard model in one dimension is given by

$$H = \sum_i [-\mu n(i) + UD(i) + Vn(i)n^\alpha(i)], \quad (1)$$

where $n(i) = c^\dagger(i)c(i)$ is the charge density operator, $c(i)$ [$c^\dagger(i)$] is the electron annihilation (creation) operator - in the spinor notation - satisfying canonical anti-commutation relations. We use the Heisenberg picture: $i = (\mathbf{i}, t)$, where \mathbf{i} stands for the lattice vector \mathbf{R}_i . The Bravais lattice is a linear chain of N sites with lattice constant a . μ is the chemical potential; U and V are the strengths of the local and intersite interactions, respectively. $D(i) = n_\uparrow(i)n_\downarrow(i) = n(i)[n(i) - 1]/2$ is the double occupancy operator. Hereafter, for a generic operator $\Phi(i)$, we shall use the following notation

$$\Phi^\alpha(i, t) = \sum_j \alpha_{ij} \Phi(j, t),$$

where α_{ij} is the projection operator over nearest neighboring sites

$$\alpha_{ij} = \frac{1}{N} \sum_k e^{ik(R_i - R_j)} \alpha(k) \quad \alpha(k) = \cos(ka),$$

and the sum is over the first Brillouin zone.

A. Eigenoperators and eigenvalues

Upon introducing the Hubbard operators $\xi(i) = [n(i) - 1]c(i)$ and $\eta(i) = n(i)c(i)$, one may define the composite

field operator

$$\psi(i) = \begin{pmatrix} \psi^{(\xi)}(i) \\ \psi^{(\eta)}(i) \end{pmatrix}, \quad (2)$$

where

$$\begin{aligned} \psi^{(\xi)}(i) &= \begin{pmatrix} \psi_1^{(\xi)}(i) \\ \psi_2^{(\xi)}(i) \\ \vdots \\ \psi_5^{(\xi)}(i) \end{pmatrix} = \begin{pmatrix} \xi(i) \\ \xi(i)[n^\alpha(i)] \\ \vdots \\ \xi(i)[n^\alpha(i)]^4 \end{pmatrix}, \\ \psi^{(\eta)}(i) &= \begin{pmatrix} \psi_1^{(\eta)}(i) \\ \psi_2^{(\eta)}(i) \\ \vdots \\ \psi_5^{(\eta)}(i) \end{pmatrix} = \begin{pmatrix} \eta(i) \\ \eta(i)[n^\alpha(i)] \\ \vdots \\ \eta(i)[n^\alpha(i)]^4 \end{pmatrix}. \end{aligned} \quad (3)$$

By exploiting the algebraic properties of the operators $n(i)$ and $D(i)$, it is easy to show that the fields $\psi^{(\xi)}(i)$ and $\psi^{(\eta)}(i)$ are eigenoperators of the Hamiltonian (1) [52]:

$$\begin{aligned} i \frac{\partial}{\partial t} \psi^{(\xi)}(i) &= [\psi^{(\xi)}(i), H] = \varepsilon^{(\xi)} \psi^{(\xi)}(i), \\ i \frac{\partial}{\partial t} \psi^{(\eta)}(i) &= [\psi^{(\eta)}(i), H] = \varepsilon^{(\eta)} \psi^{(\eta)}(i). \end{aligned} \quad (4)$$

In Eq. (4), $\varepsilon^{(\xi)}$ and $\varepsilon^{(\eta)}$ are the 5×5 energy matrices [52]

$$\varepsilon^{(\xi)} = \begin{pmatrix} -\mu & 2V & 0 & 0 & 0 \\ 0 & -\mu & 2V & 0 & 0 \\ 0 & 0 & -\mu & 2V & 0 \\ 0 & 0 & 0 & -\mu & 2V \\ 0 & -3V & \frac{25}{2}V & -\frac{35}{2}V & -\mu + 10V \end{pmatrix}, \quad (5)$$

$$\varepsilon^{(\eta)} = \begin{pmatrix} U - \mu & 2V & 0 & 0 & 0 \\ 0 & U - \mu & 2V & 0 & 0 \\ 0 & 0 & U - \mu & 2V & 0 \\ 0 & 0 & 0 & U - \mu & 2V \\ 0 & -3V & \frac{25}{2}V & -\frac{35}{2}V & U - \mu + 10V \end{pmatrix}, \quad (6)$$

whose eigenvalues, $E_m^{(\xi)}$ and $E_m^{(\eta)}$, are given by

$$\begin{aligned} E_m^{(\xi)} &= -\mu + (m-1)V, \\ E_m^{(\eta)} &= -\mu + U + (m-1)V \end{aligned} \quad \{m = 1, \dots, 5\}. \quad (7)$$

B. Retarded Green's functions and correlation functions

The knowledge of a complete set of eigenoperators and eigenenergies of the Hamiltonian allows for an exact expression of the retarded Green's function

$$\begin{aligned} G^{(s)}(t - t') &= \theta(t - t') \langle \{ \psi^{(s)}(0, t), \psi^{s\dagger}(0, t') \} \rangle \\ &= \frac{i}{(2\pi)} \int_{-\infty}^{+\infty} d\omega e^{-i\omega(t-t')} G^{(s)}(\omega), \end{aligned} \quad (8)$$

and, consequently, of the correlation function

$$\begin{aligned} C^{(s)}(t-t') &= \langle \psi^{(s)}(0, t) \psi^{(s)\dagger}(0, t') \rangle \\ &= \frac{1}{(2\pi)} \int_{-\infty}^{+\infty} d\omega e^{-i\omega(t-t')} C^{(s)}(\omega). \end{aligned} \quad (9)$$

In the above equations, $s = \xi, \eta$ and $\langle \dots \rangle$ denotes the quantum-statistical average over the grand canonical ensemble. One finds [52]

$$\begin{aligned} G^{(s)}(\omega) &= \sum_{m=1}^5 \frac{\sigma^{(s,m)}}{\omega - E_m^{(s)} + i\delta}, \\ C^{(s)}(\omega) &= \pi \sum_{m=1}^5 \sigma^{(s,m)} T_m^{(s)} \delta(\omega - E_m^{(s)}), \end{aligned} \quad (10)$$

where $T_m^{(s)} = 1 + \tanh(\beta E_m^{(s)}/2)$, $\beta = 1/k_B T$, and the spectral density matrices $\sigma^{(s,m)}$ are given by

$$\sigma^{(s,m)} = \Sigma_m^{(s)} \Gamma^{(m)}, \quad (11)$$

where $m = 1, \dots, 5$; $\Gamma^{(m)}$ are matrices of rank 5×5 :

$$\begin{aligned} \Gamma_{l,k}^{(1)} &= \delta_{l,1} \delta_{k,1}, \\ \Gamma_{l,k}^{(m)} &= \left(\frac{m-1}{2} \right)^{l+k-2}, \end{aligned}$$

where $m = 2, \dots, 5$ and the $\Sigma_m^{(s)}$ are given by

$$\begin{aligned} \Sigma_1^{(s)} &= \frac{1}{6} \left(6I_{1,1}^{(s)} - 25I_{1,2}^{(s)} + 35I_{1,3}^{(s)} - 20I_{1,4}^{(s)} + 4I_{1,5}^{(s)} \right), \\ \Sigma_2^{(s)} &= \frac{4}{3} \left(6I_{1,2}^{(s)} - 13I_{1,3}^{(s)} + 9I_{1,4}^{(s)} - 2I_{1,5}^{(s)} \right), \\ \Sigma_3^{(s)} &= -6I_{1,2}^{(s)} + 19I_{1,3}^{(s)} - 16I_{1,4}^{(s)} + 4I_{1,5}^{(s)}, \\ \Sigma_4^{(s)} &= \frac{4}{3} \left(2I_{1,2}^{(s)} - 7I_{1,3}^{(s)} + 7I_{1,4}^{(s)} - 2I_{1,5}^{(s)} \right), \\ \Sigma_5^{(s)} &= \frac{1}{6} \left(-3I_{1,2}^{(s)} + 11I_{1,3}^{(s)} - 12I_{1,4}^{(s)} + 4I_{1,5}^{(s)} \right). \end{aligned} \quad (12)$$

$I_{a,b}^{(s)}$ are the elements of the normalization matrix $I^{(s)} = \langle \{ \psi^{(s)}(i), \psi^{(s)\dagger}(i) \} \rangle$ which can be expressed as

$$\begin{aligned} I_{1,k}^{(\xi)} &= \kappa^{(k-1)} - \lambda^{(k-1)}, & \kappa^{(p)} &= \langle [n^\alpha(i)]^p \rangle, \\ I_{1,k}^{(\eta)} &= \lambda^{(k-1)}, & \lambda^{(p)} &= \frac{1}{2} \langle n(i) [n^\alpha(i)]^p \rangle. \end{aligned} \quad (13)$$

Thus, the CFs depend on the external parameters $n = \langle n(i) \rangle$, T , U , V and on the internal parameters: μ , $\kappa^{(p)}$, and $\lambda^{(p)}$. It is easy to show that the CFs obey the following self-consistent equations:

$$C_{1,k}^{(\xi)} + C_{1,k}^{(\eta)} = \kappa^{(k-1)} - \lambda^{(k-1)} \quad (k = 1, \dots, 5). \quad (14)$$

The number of these equations is not sufficient to determine all the internal parameters, and one needs other equations. This problem will be considered in the next subsection, where a self-consistent scheme, capable to compute the internal parameters, will be presented.

C. Self-consistent equations

The previous analysis shows that the complete solution of the model requires the knowledge of the parameters μ , $\kappa^{(k)}$ and $\lambda^{(k)}$. These quantities may be computed by using algebra constraints and symmetry requirements [52]. By recalling the projection nature of the Hubbard operators $\xi(i)$ and $\eta(i)$, it is easy to see that the following algebraic properties hold:

$$\begin{aligned} \xi^\dagger(i) n(i) &= 0 & \eta^\dagger(i) n(i) &= \eta^\dagger(i), \\ \xi^\dagger(i) D(i) &= 0 & \eta^\dagger(i) D(i) &= 0. \end{aligned} \quad (15)$$

These are fundamental relations and constitute the basis to construct a self-consistent procedure to compute the various unknown parameters of the solution. One first fixes an arbitrary site, say i , of the chain, then splits the Hamiltonian (1) in the sum of two terms:

$$\begin{aligned} H &= H_0(i) + H_I(i), \\ H_I(i) &= 2V n(i) n^\alpha(i), \end{aligned} \quad (16)$$

and introduce the $H_0(i)$ representation: the statistical average of any operator O can be expressed as

$$\langle O \rangle = \frac{\langle O e^{-\beta H_I(i)} \rangle_{0,i}}{\langle e^{-\beta H_I(i)} \rangle_{0,i}}, \quad (17)$$

where $\langle \dots \rangle_{0,i}$ stands for the trace with respect to the reduced Hamiltonian $H_0(i)$: i.e., $\langle \dots \rangle_{0,i} = \text{Tr}\{\dots e^{-\beta H_0(i)}\} / \text{Tr}\{e^{-\beta H_0(i)}\}$. In the following, we shall drop the index i since, by requiring translational invariance, all the sites are equivalent. As it is shown in Appendix A, the parameters $\kappa^{(k)}$ and $\lambda^{(k)}$ can be written as a function of two parameters $X_1 = \langle n^\alpha(i) \rangle_0$ and $X_2 = \langle D^\alpha(i) \rangle_0$, in terms of which one may find a solution of the model. By exploiting the translational invariance along the chain, one can impose

$$\begin{aligned} \langle n(i) \rangle &= \langle n^\alpha(i) \rangle, \\ \langle D(i) \rangle &= \langle D^\alpha(i) \rangle, \end{aligned} \quad (18)$$

finding thus two equations allowing one to determine X_1 and X_2 as functions of μ .

$$\begin{aligned} X_1 &= 2e^{\beta\mu} (1 - X_1 - dX_2) (1 + aX_1 + a^2X_2) \\ &\quad + e^{\beta(2\mu-U)} [2 + (d-1)X_1 - 2dX_2] (1 + dX_1 + d^2X_2), \\ X_2 &= e^{\beta(2\mu-U)} [1 + dX_1 - (2d+1)X_2] (1 + dX_1 + d^2X_2) \\ &\quad - 2e^{\beta\mu} (1 + d)X_2 (1 + aX_1 + a^2X_2), \end{aligned} \quad (19)$$

where $a = e^{-\beta V} - 1$ and $d = e^{-2\beta V} - 1$. The chemical potential μ can be determined by means of the equation

$$\begin{aligned} n &= \frac{1}{\Xi} [(X_1 - 2X_2)(1 + aX_1 + a^2X_2) \\ &\quad + 2X_2(1 + dX_1 + d^2X_2)], \end{aligned} \quad (20)$$

where $\Xi = 1 - X_1 + X_2 + (X_1 - 2X_2)(1 + aX_1 + a^2X_2) + X_2(1 + dX_1 + d^2X_2)$. Thus Eqs. (19) and (20) constitute a set of coupled equations allowing one to ascertain the three parameters μ , X_1 , and X_2 in terms of the external parameters of the model (n , U , V , and T). Once these quantities are known, all the properties of the model can be computed. In particular, the local CFs can be expressed in terms of the parameters $D = \langle D(i) \rangle$, $\kappa^{(p)}$, and $\lambda^{(p)}$, defined in Eq. (13), and $\pi^{(p)} = \langle [D^\alpha(i)]^p \rangle$, $\delta^{(p)} = \langle n(i)[D^\alpha(i)]^p \rangle / 2$, $\theta^{(p)} = \langle D(i)[D^\alpha(i)]^p \rangle / 2$. Indeed, it is easy to derive the following relations for the two-point correlation functions

$$\begin{aligned} \langle n(i)n(i+1) \rangle &= 2\lambda^{(1)} \\ \langle n(i)n(i+2) \rangle &= 2\kappa^{(2)} - n - 2D \\ \langle n(i)D(i+1) \rangle &= 2\delta^{(1)} \\ \langle n(i)D(i+2) \rangle &= \frac{2}{3}\kappa^{(3)} - \kappa^{(2)} + \frac{1}{3}n \\ \langle D(i)D(i+1) \rangle &= 2\theta^{(1)} \\ \langle D(i)D(i+2) \rangle &= 2\pi^{(2)} - D, \end{aligned} \quad (21)$$

and for the three-point correlation functions

$$\begin{aligned} \langle n(i)n(i+1)n(i+2) \rangle &= 4\lambda^{(2)} - 2\lambda^{(1)} - 4\delta^{(1)} \\ \langle n(i)n(i+1)D(i+2) \rangle &= \frac{4}{3}\lambda^{(3)} - 2\lambda^{(2)} + \frac{2}{3}\lambda^{(1)} \\ \langle D(i)n(i+1)D(i+2) \rangle &= 4\delta^{(2)} - 2\delta^{(1)} \\ \langle D(i)D(i+1)D(i+2) \rangle &= 4\theta^{(2)} - 2\theta^{(1)}. \end{aligned} \quad (22)$$

The double occupancy, in terms of X_1 and X_2 , is given by

$$D = \frac{1}{\Xi} [X_2(1 + dX_1 + d^2X_2)]. \quad (23)$$

In Appendix A we show how the parameters $\kappa^{(p)}$, $\lambda^{(p)}$, $\pi^{(p)}$, $\delta^{(p)}$, $\theta^{(p)}$ can be expressed in terms of the two basic parameters X_1 and X_2 . At half filling, the system of equations (19) and (20) can be solved analytically and one has

$$\mu = \frac{1}{2}U + 2V, \quad (24)$$

$$\begin{aligned} X_1 &= 1 - \frac{1}{4GK(K-1)} \{ (K+1)[1 + 2GK + K^2 \\ &\quad - \sqrt{(1 + 2GK + K^2)^2 - 8GK(K-1)^2}] \}, \\ X_2 &= \frac{1}{4GK(K-1)^2} \{ 1 + 2GK + K^2 \\ &\quad - \sqrt{(1 + 2GK + K^2)^2 - 8GK(K-1)^2} \}, \end{aligned} \quad (25)$$

where $K = e^{-\beta V}$ and $G = e^{\beta U/2}$. As a consequence, one finds

$$\begin{aligned} D &= \frac{1}{2 + 2G(1 - a^2X_2)^2} \\ \lambda^{(1)} &= \frac{1 - 2a^2X_2 + (1 - 4K + 2K^2 + K^4)X_2^2}{2[1 - 2a^2X_2 + a^2(1 + K^2)X_2^2]}. \end{aligned} \quad (26)$$

D. Nonlocal correlation functions

We shall now consider the problem of computing non-local correlation functions $\langle O_1(i)O_2(j) \rangle$, where $O_1(i)$ and $O_2(j)$ are generic operators and j is a site m steps ($m \geq 1$) away from the site i . To compute these quantities one needs only to know the local correlators (21) thanks to some recurrence relations. We refer the interested reader to Appendix B for analytical details. In particular, for the charge and double occupancy correlation functions, one finds

$$\begin{aligned} \langle n(i)n(j) \rangle &= n^2 + Ap^{|i-j|} + Bq^{|i-j|}, \\ \langle D(i)D(j) \rangle &= D^2 + Cp^{|i-j|} + Eq^{|i-j|}, \end{aligned} \quad (27)$$

where the coefficients A , B , C , E , and the exponents p and q - all defined in Appendix B - are functions only of the short-range correlation functions $\lambda^{(1)}$, $\kappa^{(2)}$, $\theta^{(1)}$, and $\pi^{(2)}$.

E. Density of states

By noting that the cross GFs $\langle \psi^{(\xi)}(i, t)\psi^{(\eta)\dagger}(i, t) \rangle$ vanish, the electronic density of states (DOS) is given by

$$\begin{aligned} N(\omega) &= \left(-\frac{1}{\pi}\right) \text{Im}[G_{11}^{(\xi)}(\omega) + G_{11}^{(\eta)}(\omega)] \\ &= \sum_{m=1}^5 [\Sigma_m^{(\xi)}\delta(\omega - E_m^{(\xi)}) + \Sigma_m^{(\eta)}\delta(\omega - E_m^{(\eta)})]. \end{aligned} \quad (28)$$

As one can immediately see, the DOS is a sum of delta's functions weighted by the corresponding $\Sigma_m^{(s)}$'s. It is worthwhile to observe that the expressions of the $\Sigma_m^{(s)}$'s (12) lead to the following sum rule:

$$\sum_{n=1}^5 [\Sigma_n^{(\xi)} + \Sigma_n^{(\eta)}] = \int_{-\infty}^{+\infty} d\omega N(\omega) = 1. \quad (29)$$

In the following, we shall use a Lorentzian broadening for the delta functions $\delta(\omega - \omega_0) = \varepsilon / [(\omega - \omega_0)^2 + \varepsilon^2]\pi$ with $\varepsilon = 0.1$.

F. Summary

Summarizing, in this section we have shown that the model can be exactly solved by using the Green's function formalism and the equation of motion method. The central point in this approach lies in the fact that there exists a closed set of eigenoperators of the Hamiltonian (1) [see Eqs. (4)] allowing for an exact determination of the correlation functions, as it is shown in Secs. II B, II D and in the Appendices. Exact expressions for the GFs and CFs can be written in terms of few local correlators. By using algebraic properties of the relevant operators and

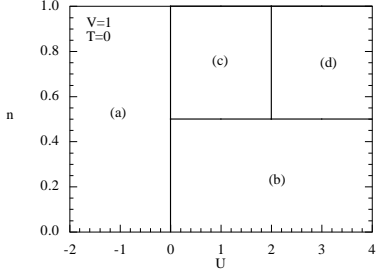


FIG. 1: The phase diagram in the plane (U, n) at $T = 0$ and $V = 1$. One can identify four phases.

symmetry properties, these correlators can be expressed in terms of the chemical potential μ and of the parameters X_1 and X_2 . These three quantities are determined as functions of the external parameters n , U , V and T by solving the system of equations (19) and (20). Once these quantities are known, all properties of the model can be computed. In the next section we shall present a comprehensive study of the properties of the system at zero-temperature.

III. ZERO TEMPERATURE RESULTS

In this section we derive the phase diagram of the AL-EHM in the (U, n) plane. More specifically, we shall numerically solve the set of equations (19) and (20) at $T = 0$ and study the behavior of relevant correlation functions and of the density of states in order to envisage the distribution of the particles for different densities. The results obtained are displayed in Fig. 1: one may distinguish four different phases, according to the values of the internal parameters.

Phase (a). The phase (a) is observed in the region $(0 \leq n \leq 1, U < 0)$ and is characterized by the following values of the parameters:

$$\begin{aligned} X_1 &= \frac{2n}{2-n}, & \kappa^{(3)} &= \frac{2n(1+n)}{2-n}, & A &= (2-n)n, \\ X_2 &= \frac{n}{2-n}, & \kappa^{(4)} &= \frac{2n(1+3n)}{2-n}, & B &= E = 0, \\ D &= n/2, & \pi^{(2)} &= \frac{n}{2(2-n)}, & C &= \frac{(2-n)n}{4}, \\ \kappa^{(2)} &= \frac{2n}{2-n}, & \lambda^{(k)} &= \theta^{(1)} = 0, & p &= -\frac{n}{2-n}, \\ & & & & q &= 0. \end{aligned}$$

The chemical potential takes the value $U/2$ for $n < 1$, whereas at $n = 1$ one naturally finds $\mu = 2V + U/2$. The attractive on-site potential favors the formation of doubly occupied sites. At the same time, the repulsive intersite potential disfavors the occupation of neighboring sites. The expectation values $D = n/2$ and $\langle n(i)[n^\alpha(i)]^k \rangle = 0$

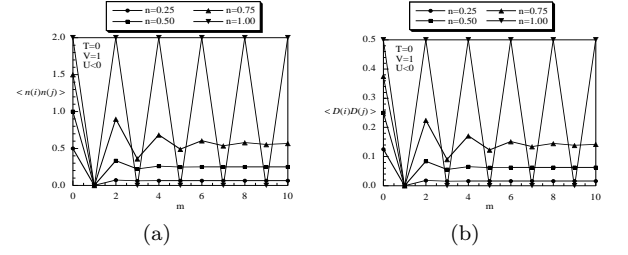


FIG. 2: The charge (a) and the double occupancy (b) correlation functions as functions of the distance $m = |i - j|$ for $U < 0$, $V = 1$ and $n=0.25, 0.5, 0.75, 1$.

suggest that, in the thermodynamic limit, there are neither singly occupied sites nor neighboring sites occupied. For $n < 1$ one does not find any charge ordered state and the energy necessary to add two electrons is $2\mu = U$. At half filling ($n = 1$), the chemical potential jumps from the value $\mu = U/2$ to the value $\mu = 2V + U/2$, as required by particle-hole symmetry. Indeed, one needs to provide an energy amount of $2V$ for an extra electron to occupy a nearest neighbor site. At $n = 1$ half of the sites are doubly occupied: by varying the particle density, the system undergoes a PT to an ordered state characterized by a checkerboard distribution of doubly occupied sites. This can be clearly seen in Figs. 2a-b, where we plot the correlation functions

$$\begin{aligned} \langle n(i)n(j) \rangle &= n^2 + n(2-n)(-1)^m e^{-m/\xi_n}, \\ \langle D(i)D(j) \rangle &= D^2 + \frac{n(2-n)}{4}(-1)^m e^{-m/\xi_n} \end{aligned} \quad (30)$$

as a function of the distance $m = |i - j|$. At half filling, both CFs present a two-site periodicity. The correlation length ξ_n in Eqs. (30) is defined as

$$\xi_n = \left[\ln \left(\frac{1}{|p|} \right) \right]^{-1}. \quad (31)$$

When $n < 1$ the parameter $|p|$ is less than 1. Thus, the CFs (30) decrease exponentially, oscillating around the ergodic values n^2 and D^2 , respectively. On the other hand, at half filling $|p| = 1$: the correlation length diverges, a long-range order is established, and both CFs present a two-site periodicity.

The distribution of the particles in the phase (a) is shown in Fig. 3, where we report just one possible configuration. The configurations in the ground state will have no doubly occupied sites next to each other. When

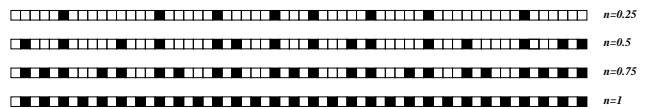


FIG. 3: Distribution of the particles along the chain by varying the particle density at $T = 0$ and $U < 0$. White and black squares denote empty and doubly occupied sites, respectively.

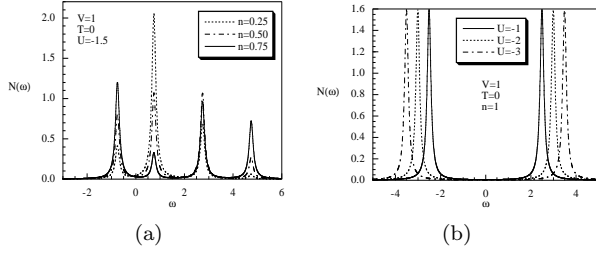


FIG. 4: (a) The density of states at zero temperature, $V = 1$ and $U = -1.5$ is reported as a function of the frequency for $n = 0.25, 0.5$ and 0.75 . (b) The density of states at zero temperature, $V = 1$ and $n = 1$ is reported as a function of the frequency for $U = -1, -2$ and -3 .

$n < 1$, there is no ordered pattern in the distribution of the particles, whereas, for $n = 1$, one observes the well-known checkerboard distribution of doubly occupied sites [18]. In Figs. 4a-b, we plot the density of states at zero temperature and attractive U , for $n < 1$ and $n = 1$, respectively. For $n < 1$, the DOS exhibits four peaks at energies $E_1^{(\eta)} = U/2$, $E_1^{(\xi)} = -U/2$, $E_3^{(\xi)} = -U/2 + 2V$, $E_5^{(\xi)} = -U/2 + 4V$: the electrons can occupy only states with these associated energies. For $n = 1$, the excitation spectrum contains only two allowed values, leading to a DOS with two peaks at $E_1^{(\eta)} = U/2 - 2V$, and $E_5^{(\xi)} = -U/2 + 2V$. By varying the particle density, the weights of the peaks change as

$$\begin{aligned} \Sigma_1^{(\eta)} &= \frac{n}{2} & \Sigma_1^{(\xi)} &= \frac{2(1-n)^2}{2-n} \\ \Sigma_3^{(\xi)} &= \frac{2n(1-n)}{2-n} & \Sigma_5^{(\xi)} &= \frac{n^2}{2(2-n)}. \end{aligned}$$

The weights relative to the other energies are zero: $\Sigma_2^{(\xi)} = \Sigma_4^{(\xi)} = \Sigma_2^{(\eta)} = \Sigma_3^{(\eta)} = \Sigma_4^{(\eta)} = \Sigma_5^{(\eta)} = 0$.

Phase (b). The phase (b) is observed in the region ($0 \leq n \leq 0.5$, $U > 0$) and is characterized by the following values of the parameters

$$\begin{aligned} X_1 &= \frac{n}{1-n}, & \kappa^{(2)} &= \frac{n}{2(1-n)}, & A &= n(1-n), \\ X_2 &= D = 0, & \kappa^{(3)} &= \frac{n(1+2n)}{4(1-n)}, & B &= E = C = 0, \\ \pi^{(2)} &= \theta^{(1)} = 0, & p &= -\frac{n}{1-n}, \\ \lambda^{(k)} &= 0, & \kappa^{(4)} &= \frac{n(1+6n)}{8(1-n)}, & q &= 0. \end{aligned}$$

and

$$\mu = \begin{cases} 0 & (n < 0.5) \\ U & (n = 0.5 \text{ and } 0 < U < 2V) \\ 2V & (n = 0.5 \text{ and } U > 2V). \end{cases}$$

The repulsion between electrons on the same site and on neighboring sites, leads to a scenario where the electrons will tend to singly occupy non-neighbor sites, as confirmed by the expectation values $D = 0$ and

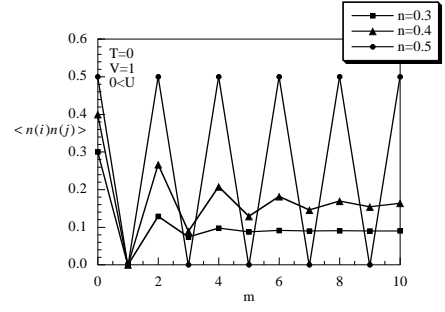


FIG. 5: The charge correlation function $\langle n(i)n(j) \rangle$ for $U > 0$ is reported as a function of the distance $m = |i - j|$ at $T = 0$, $V = 1$ and $n = 0.3, 0.4$ and 0.5 .

$\langle n(i)[n^\alpha(i)]^k \rangle = 0$. For particle densities less than quarter filling, i.e., $n < 0.5$, there is no cost in energy to add one electron, thus $\mu = 0$. At quarter filling, one has to distinguish two cases: (i) when $0 < U < 2V$, the chemical potential jumps from the value $\mu = 0$ to the value $\mu = U$; (ii) for $U > 2V$, the chemical potential presents a jump from $\mu = 0$ to $\mu = 2V$. As a result, for $n > 0.5$, as illustrated in Fig. 1, there are two distinct phases, (c) and (d). When $0 < U < 2V$, by adding one electron the system enters phase (c), characterized by the presence of both singly and doubly occupied sites. The minimization of the energy leads to a cost in energy of $\mu = U$ to accommodate an extra electron. On the other hand, when $U > 2V$, by adding one electron, the system is driven into phase (d), characterized by the presence of neighbor arbitrary-spin singly occupied sites, requiring thus an energy cost of $\mu = 2V$.

Right at quarter filling, half of the sites are singly occupied: by varying the particle density, the system undergoes a PT to an ordered state characterized by a checkerboard distribution of arbitrary-spin singly occupied sites. This is clearly shown in Fig. 5, where we plot the charge correlation function $\langle n(i)n(j) \rangle = n^2 + n(1-n)(-1)^m e^{-m/\xi_n}$ as a function of the relative distance: when $n < 0.5$ one finds that the parameter $|p|$ appearing in Eq. (27) is less than 1. As a result, $\langle n(i)n(j) \rangle$ decreases exponentially, oscillating around the ergodic value n^2 . At quarter filling one finds $|p| = 1$: the correlation length (31) diverges and a long-range order is established, as evidenced by the two-site periodicity of $\langle n(i)n(j) \rangle$.

The DOS at zero temperature and repulsive U is shown in Fig. 6a for $n < 0.5$. In Fig. 6b we plot the DOS at $n = 0.5$ for $U < 2V$ (continuous line) and $U > 2V$ (dotted line). For $n < 0.5$, the DOS exhibits four peaks at the energies $E_1^{(\eta)} = U$, $E_1^{(\xi)} = 0$, $E_2^{(\xi)} = V$, $E_3^{(\xi)} = 2V$. For $n = 0.5$ and $0 < U < 2V$, the electrons can occupy only three states at the energies $E_1^{(\eta)} = 0$, $E_1^{(\xi)} = -U$, $E_3^{(\xi)} = -U + 2V$. For $n = 0.5$ and $U > 2V$, the DOS still exhibits three peaks but now at the energies $E_1^{(\eta)} = U - 2V$, $E_1^{(\xi)} = -2V$, $E_3^{(\xi)} = 0$. By varying n the weights

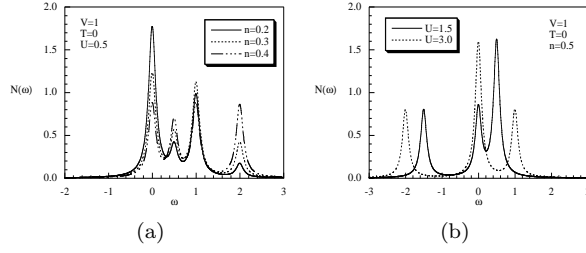


FIG. 6: The density of states $N(\omega)$ as a function of the frequency ω at zero temperature, $V = 1$ and (a) $U = 1/2$ for $n=0.2, 0.3$ and 0.4 ; (b) $n = 0.5$, for $U = 3/2$ and 3 .

of the peaks change as

$$\begin{aligned} \Sigma_1^{(\eta)} &= \frac{n}{2} & \Sigma_1^{(\xi)} &= \frac{2 - 7n(1 - n)}{2(1 - n)} \\ \Sigma_2^{(\xi)} &= \frac{2n(2n - 1)}{1 - n} & \Sigma_3^{(\xi)} &= \frac{n^2}{1 - n}. \end{aligned}$$

The weights relative to the other energies are zero.

Phase (c) The phase (c) is observed in the region ($0.5 \leq n \leq 1$, $0 < U < 2V$) and is characterized by the following values of the parameters:

$$\begin{aligned} X_1 &= 2n, & \kappa^{(2)} &= \frac{1}{2}(2n^2 + 3n - 1), \\ X_2 &= 2n - 1, & \kappa^{(3)} &= \frac{1}{4}(18n^2 + n - 3), \\ D &= n - 1/2, & \kappa^{(4)} &= \frac{1}{8}(110n^2 - 45n - 1), \\ \pi^{(2)} &= n(n - 1/2), & \lambda^{(k)} &= \theta^{(1)} = 0, \end{aligned}$$

and

$$\begin{aligned} A &= n^2, \\ B &= E = -2n^2 + 3n - 1, & p &= -1, \\ C &= (n - 1/2)^2, & q &= 0. \end{aligned}$$

The chemical potential takes the value U for $0.5 \leq n < 1$ and $2V + U/2$ at $n = 1$. The repulsive on-site and intersite potentials force the electrons to prefer seating at different sites and disfavor the occupation of neighboring sites. However, when the intersite interaction dominates the on-site one, the minimization of the energy requires the extra electrons above $n = 0.5$ to occupy nonempty sites. This situation is well described by the expectation values $D = n - 1/2$ and $\langle n(i)[n^\alpha(i)]^k \rangle = 0$. Thus, in the thermodynamic limit, there can be singly and doubly occupied sites and no neighboring sites are filled. By increasing n , the number of doubly occupied sites increases linearly. In this region, the correlation length (31) diverges: one finds a charge ordered state characterized by a checkerboard distribution of alternating empty and occupied (either singly or doubly) sites. For $n < 1$ the energy necessary to add one electron is $\mu = U$. Upon increasing the particle density, at half filling the checkerboard distribution is realized with only doubly occupied

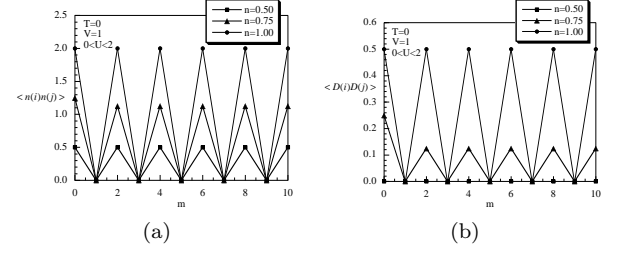


FIG. 7: The charge (a) and the double occupancy (b) correlation functions as functions of the distance $m = |i - j|$ at $T = 0$, $V = 1$ and $n = 0.5, 0.75$ and 1 .

sites alternating with empty ones and, correspondingly, the chemical potential jumps from the value $\mu = U$ to the value $\mu = 2V + U/2$. Since all the nonempty sites are already doubly occupied, an extra electron would go to occupy an empty site with a cost in energy of $2V$. The existence of the ordered states is endorsed by the behavior of the charge and double occupancy CFs.

$$\begin{aligned} \langle n(i)n(i+m) \rangle &= n^2[1 + (-1)^m] \\ \langle D(i)D(i+m) \rangle &= D^2[1 + (-1)^m] \quad m \geq 1 \end{aligned}$$

and reported in Figs. 7a and 7b. One clearly observes a two-site periodicity of $\langle n(i)n(i+m) \rangle$ and $\langle D(i)D(i+m) \rangle$, leading to an ordered charge distribution: one every two sites is at least singly occupied. The double periodicity of the double occupancy CF is, of course, to be understood as an average over all the possible distributions of doubly occupied sites that are, of course, energetically equivalent.

The distribution of the particles in the region ($0 \leq n \leq 1$, $0 < U < 2V$) is drawn in Fig. 8, where we represent just one possible configuration. At quarter filling the ground states of the Hamiltonian are checkerboard configurations where empty sites alternate with sites occupied by one particle of arbitrary spin. By increasing n , the charge order persists and one observes an increase of the number of doubly occupied sites, as illustrated in Fig. 8. Finally, at half filling, one observes a checkerboard distribution of doubly occupied sites [24]. The density of states at zero temperature is plotted in Fig. 9a for $0.5 < n < 1$ and $U = V/2$ and in Fig. 9b for $n = 1$ and different values of U . One observes that, when $n < 1$, the DOS exhibits five peaks at the energies $E_1^{(\eta)} = 0$, $E_1^{(\xi)} = -U$, $E_3^{(\xi)} = -U + 2V$,

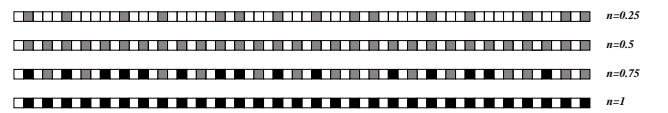


FIG. 8: Distribution of the particles along the chain by varying the particle density at $T = 0$ and $0 < U < 2V$. White and black squares denote empty and doubly occupied sites, respectively. Grey squares denote arbitrary-spin singly occupied sites.

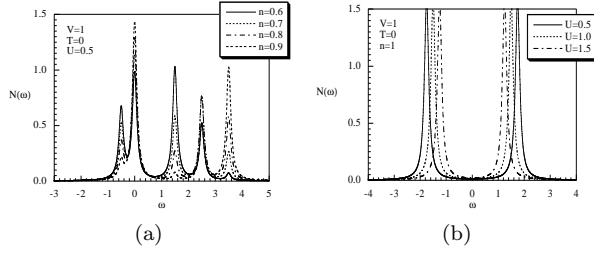


FIG. 9: The density of states $N(\omega)$ as a function of the frequency ω at zero temperature, $V = 1$ and (a) $U = 1/2$ for $n = 0.6, 0.7, 0.8, 0.9$; (b) $n = 1$, for $U = 1/2, 1$ and $3/2$.

$E_4^{(\xi)} = -U + 3V$, $E_5^{(\xi)} = -U + 4V$. For $n = 1$ and $0 < U < 2V$, the DOS exhibits only two peaks at the energies $E_1^{(\eta)} = -U/2 - 2V$, $E_5^{(\xi)} = -U/2 + 2V$. By varying n the weights of the peaks change as

$$\begin{aligned} \Sigma_1^{(\xi)} &= \frac{1}{2}(1-n) & \Sigma_5^{(\xi)} &= \frac{1}{2}(1-2n)^2 \\ \Sigma_3^{(\xi)} &= 2(1-n)^2 & \Sigma_1^{(\eta)} &= \frac{n}{2} \\ \Sigma_4^{(\xi)} &= -2 + 6n - 4n^2. \end{aligned}$$

The weights relative to the other energies are zero.

Phase (d) The phase (d) is observed in the region ($0.5 \leq n \leq 1$, $U > 2V$) and is characterized by the following values of the parameters,

for $0.5 \leq n < 1$

$$\begin{aligned} \mu &= 2V, & \lambda^{(1)} &> \lambda^{(2)} > \lambda^{(3)} > \lambda^{(4)}, \\ X_1 &= 1, & A &= (1-n)n, \\ X_2 &= 0, & B &= C = E = 0, \\ D &= 0, & p &= -(1-n)/n, \\ \kappa^{(2)} &> \kappa^{(3)} > \kappa^{(4)}, & q &= 0, \end{aligned}$$

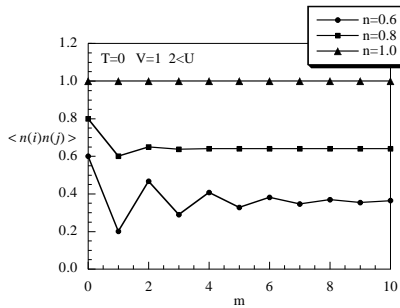


FIG. 10: The charge correlation function $\langle n(i)n(j) \rangle$ for $U > 2V$ as a function of the distance $m = |i - j|$ at $T = 0$, $V = 1$ and $n = 0.6, 0.8$ and 1 .

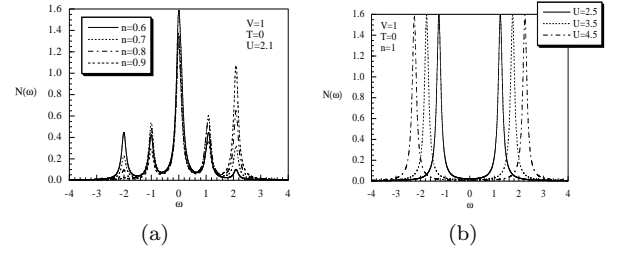


FIG. 11: The density of states $N(\omega)$ as a function of the frequency ω at zero temperature, $V = 1$ and (a) $U = 2.1$ for $n = 0.6, 0.7, 0.8, 0.9$; (b) $n = 1$, for $U = 5/2, 7/2$ and $U = 9/2$.

and for $n = 1$,

$$\begin{aligned} \mu &= 2V + U/2 & \kappa^{(k)} &= 1, & A &= B = 0, \\ X_1 &= 1, & \pi^{(2)} &= 0, & C &= E = 0, \\ X_2 &= 0, & \lambda^{(k)} &= 1/2, & p &\neq 0, \\ D &= 0, & \theta^{(1)} &= 0, & q &\neq 0. \end{aligned}$$

In this region the on-site interaction dominates the intersite one. The minimization of the energy requires the electrons not to be paired and allows for the occupation of neighboring sites: $D = 0$ and $\langle n(i)[n^\alpha(i)]^k \rangle \neq 0$. For $n < 1$ the energy necessary to add one electron is $\mu = 2V$. At half filling the chemical potential jumps from the value $\mu = 2V$ to $\mu = 2V + U/2$. This is because an extra electron would go to occupy a singly occupied site, requiring thus an energy equal to U . The behavior of the charge correlation function is reported in Fig. 10 as a function of the relative distance. One observes that increasing the particle density, $\langle n(i)n(j) \rangle$ becomes more and more uniform losing the two-site periodicity peculiar of the region $0 < U < 2V$. At half filling the system presents an homogeneous distribution, with all singly occupied sites [24].

The density of states at zero temperature and $U > 2V$ is plotted in Fig. 11a for $0.5 < n < 1$ and in Fig. 11b for $n = 1$ and different values of U ($U > 2V$). For $n < 1$, the DOS exhibits five peaks at the energies $E_1^{(\xi)} = -2V$, $E_2^{(\xi)} = -V$, $E_3^{(\xi)} = 0$, $E_2^{(\eta)} = U - V$, $E_3^{(\eta)} = U$. For $n = 1$, the electrons can occupy two states at the energies $E_3^{(\xi)} = -U/2$, $E_3^{(\eta)} = U/2$. The distribution of the particles in the region ($0 \leq n \leq 1$, $U > 2V$) is presented in Fig. 12, where just one possible configuration



FIG. 12: Distribution of the particles along the chain by varying the particle density at $T = 0$ and $U > 2V$. White and grey squares denote empty and arbitrary spin singly occupied sites, respectively.

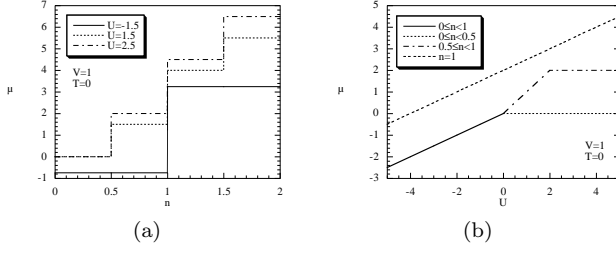


FIG. 13: (a) The chemical potential μ as a function of the particle density for $V = 1$, $T = 0$ and $U = -1.5, 1.5$ and 2.5 . (b) The chemical potential as a function of the on-site potential U for $V = 1$, $T = 0$ in the region $0 \leq n \leq 1$.

is shown. As one can clearly see, in region (d) there are no charge ordered states but at $n = 0.5$.

One can now investigate some thermodynamic quantities, whose behavior can also be relevant to ascertain some of the results previously obtained. In particular, we shall investigate the behavior of the chemical potential and of the double occupancy as a function of the particle density and of the on-site potential. In the former case, we shall consider the full range $0 \leq n \leq 2$ to better recognize the peculiar behaviors of μ and D . In Fig. 13a we plot the chemical potential as a function of n for different values of U : μ exhibits plateaus and discontinuities. In particular, (i) for $U < 0$, μ takes the constant value $\mu = U/2$ in the region $0 < n < 1$, corresponding to phase (a). At $n = 1$ there is a discontinuity corresponding to the PT to a checkerboard distribution of doubly occupied sites; (ii) for $0 < U < 2V$, μ takes the constant value $\mu = 0$ in the range $0 < n < 0.5$, corresponding to phase (b). At $n = 0.5$ there is a discontinuity corresponding to the phase transition to the checkerboard distribution of singly occupied sites. In the range $0.5 < n < 1$, μ takes the constant value $\mu = U$, corresponding to phase (c). At $n = 1$ there is a discontinuity corresponding to the PT to the checkerboard distribution of doubly occupied sites; (iii) for $U > 2V$, μ takes the constant value $\mu = 2V$ in the region $0.5 < n < 1$, corresponding to phase (d). At $n = 1$ there is a discontinuity corresponding to the PT to the homogeneous distribution of singly occupied sites. When plotted as a function of U [see Fig. 13b], the chemical potential shows a linear behavior for $n = 1$, as required by the particle-hole symmetry. For all other values of the filling, μ presents a linear behavior for attractive on-site interaction. Then, for positive U , μ presents a plateau ($\mu = 0$) when $n < 0.5$, whereas, for $0.5 \leq n < 1$, it increases linearly with U up to $U = 2V$, where it takes the constant value $\mu = 2V$. As it is evident in Fig. 14a, the double occupancy shows three different behaviors according to the value of U . For $0 \leq n \leq 1$, the double occupancy is always zero when $U > 2V$, it shows a linear behavior for negative values of U and presents a discontinuity at quarter filling, when $0 < U < 2V$. In Fig. 14b we plot the double occupancy as a function of the on-site potential U for several values of n : one observes a one-step or a two-step behavior depending on the particle density.

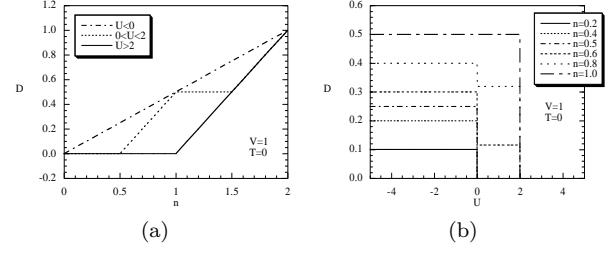


FIG. 14: (a) The double occupancy as a function of the particle density for $V = 1$, $T = 0$, $U < 0$ (dot-dashed line), $0 < U < 2V$ (dotted line) and $U > 2V$ (continuous line). (b) The double occupancy as a function of the on-site potential U for $V = 1$, $T = 0$ and various values of n .

In closing this section, it is worthwhile to mention that at zero temperature all the phases (with the exception of the case $n = 1$ and $U < 2V$) exhibit a macroscopic degeneracy growing exponentially with the volume of the lattice.

IV. FINITE TEMPERATURE RESULTS

In this section we shall investigate the finite temperature properties of the AL-EHM. We study the behavior of the system as a function of the parameters n , T , and U and again we take $V = 1$ as the unit of energy. We shall focus our attention on several thermodynamic quantities: namely, the chemical potential μ , the double occupancy D , the nearest-neighbor charge correlation $\chi^\alpha = 2\lambda^{(1)} = \langle n(i)n^\alpha(i) \rangle$, the thermal compressibility $\kappa^{(T)} = (1/n^2) \cdot dn/d\mu$, the density of states, the charge $\langle n(i)n(j) \rangle$ and double occupancy $\langle D(i)D(j) \rangle$ correlation functions, the charge χ_c and the spin χ_s susceptibilities, the internal energy $E = UD + V\chi^\alpha$, the specific heat $C = dE/dT$, and the entropy S . Under the transformation $n \rightarrow 2 - n$, these quantities transform as:

$$\begin{aligned}
 \mu(2-n) &= 4V + U - \mu(n) \\
 D(2-n) &= 1 - n + D(n) \\
 \chi^\alpha(2-n) &= 4(1-n) + \chi^\alpha(n) \\
 \chi_c(2-n) &= \chi_c(n) \\
 \chi_s(2-n) &= \chi_s(n) \\
 E(2-n) &= (U + 4V)(1-n) + E(n) \\
 C(2-n) &= C(n).
 \end{aligned} \tag{32}$$

Therefore, unless otherwise stated, we shall limit the analysis to the range $0 \leq n \leq 1$. In order to characterize the various features of the thermodynamic quantities, in the following we shall distinguish three intervals along the U line (at the borders of which zero temperature transitions occur): namely, $U < 0$, $0 < U < 2V$, and $U > 2V$.

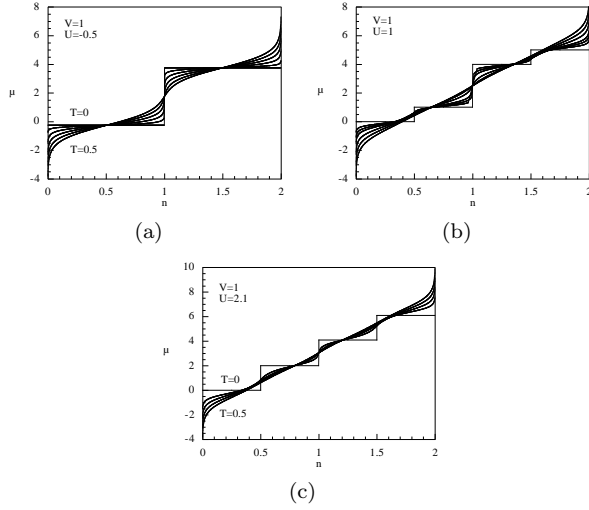


FIG. 15: The chemical potential μ as a function of the particle density n for various temperatures and (a) $U < 0$, (b) $0 < U < 2V$, (c) $U > 2V$.

A. The chemical potential

The behavior of the chemical potential as a function of the particle density n is reported in Figs. 15a-c as the temperature varies, for the three regions $U < 0$, $0 < U < 2V$ and $U > 2V$, respectively. One can immediately see that μ is always an increasing function of n , hinting at a thermodynamically stable system for all ranges of the parameters n , T , and U . We consider the full range $0 \leq n \leq 2$ to better appreciate the jumps in μ as the particle density is varied. An interesting feature is the presence of crossing points in the chemical potential curves, when plotted for different temperatures and $U < 2V$. More precisely, one observes crossing points at the values $n = 0.5$, $n = 1$, and $n = 1.5$, where PTs are observed at $T = 0$. In between these values, for temperatures close to zero, the chemical potential presents plateaus. In Sec. IV H we shall see that nearly universal crossing points are also exhibited by the specific heat. The value $n = 0.5$ is a turning point for the derivative $d\mu/dT$: for $n < 0.5$ ($n > 0.5$), μ is a decreasing (increasing) function of T . In Fig. 16 we show the chemical potential as a function of the on-site interaction U for $n = 0.25, 0.5, 0.75$ and for two temperatures. For negative U , μ increases by increasing U following approximately a linear law ($\mu = U/2$ for $T = 0$). When $U > 0$, μ deviates from the linear behavior and, for $U \approx 2V$, tends to a constant value depending both on n and T . The latter behavior has been observed also for the 2D Hubbard model (see Ref. [60] and references therein).

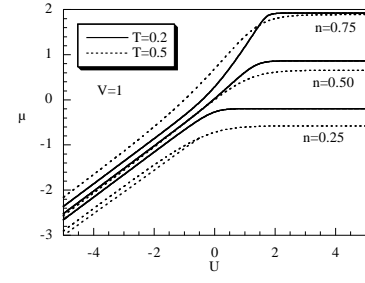


FIG. 16: The chemical potential μ as a function of the on-site interaction U for $n = 0.25, 0.5, 0.75$ and for $T = 0.2$ (solid line) and $T = 0.5$ (dotted line).

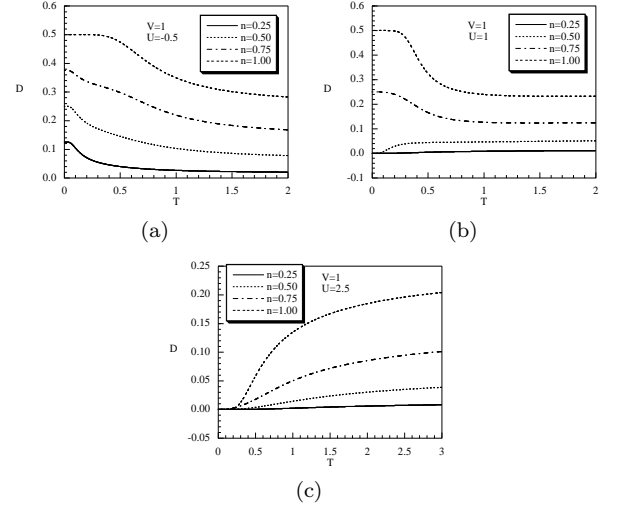


FIG. 17: The double occupancy as a function of the temperature for different values of the particle density and (a) $U = -1/2$, (b) $U = 1$, (c) $U = 5/2$.

B. The double occupancy

In Figs. 17a-c the temperature dependence of the double occupancy D is shown for the three regions $U < 0$, $0 < U < 2V$ and $U > 2V$, respectively. In the first region (attractive U), D is always a decreasing function of the temperature since the thermal excitations tend to break the doublons, i.e., the charge carriers of doubly occupied sites. In the second region ($0 < U < 2V$), the double occupancy is an increasing (decreasing) function for $n < 0.5$ ($n > 0.5$). This is easily understandable if one thinks of the zero-temperature scenario: for filling less than one-quarter, the thermal excitations may favor the formation of doublons, against the repulsive interaction U . For filling greater than one-quarter, the thermal excitations may favor the formation of neighboring singly occupied sites, against the repulsive interaction V . In the third region ($U > 2V$), the double occupancy is always an increasing function of T , since the thermal excitations favor the formation of doublons, against the repulsive interaction U . A similar behavior of the double occupancy

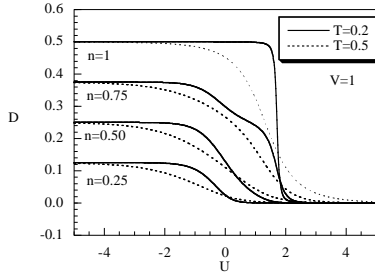


FIG. 18: The double occupancy as a function of the on-site interaction U for $n = 0.25, 0.5, 0.75, 1$ and for two different temperatures.

by varying the temperature has been found in a strong coupling analysis of the EHM at half filling [42].

It is interesting to plot the double occupancy as a function of the on-site potential U . As expected, at all temperatures, D is always a decreasing function of U . As one can see from Fig. 18, the discontinuities observed at zero temperature for $U = 0$ and $U = 2V$ are more and more smoothed as the temperature is increased. In the limit $U \rightarrow -\infty$ the double occupancy tends to the constant value $D = n/2$, independently of the temperature: all the electrons are paired. In the opposite limit, namely $U \rightarrow \infty$, the on-site repulsion prevents the double occupations of the sites.

C. The nearest-neighbor charge correlation function

As discussed in Sec. III, there are two interesting quantities which mainly characterizes the state of the system: one is the double occupancy, discussed in the previous subsection, the other is the nearest-neighbor charge correlation function $\chi^\alpha = \langle n(i)n^\alpha(i) \rangle = 2\lambda^{(1)}$. The behavior of χ^α as a function of the temperature is shown in Figs. 19a-c, for the three regions $U < 0$, $0 < U < 2V$ and $U > 2V$, respectively. As one would have expected, the behavior of χ^α is opposite to the one of D in some regions of the parameters: for instance, for attractive on-site interactions, thermal excitations tend to break the doublons and to consequently favor the occupation of neighboring sites. For $U < 2V$, χ^α is always an increasing function of T and vanishes in the limit $T \rightarrow 0$, where occupation of neighbor sites is clearly disfavored. As one can see in Figs. 19a-c, the thermal excitations may favor the occupation of neighboring sites and, in the limit $T \rightarrow \infty$, χ^α tends to the value n^2 for all values of U and n . When the on-site potential is greater than $2V$, the behavior of χ^α depends on the filling: it is an increasing (decreasing) function for $n < 0.5$ ($n > 0.5$) at low temperatures. This different behavior can be understood if one looks at Fig. 12: it is clear that for lower fillings thermal excitations are more effective in augmenting the nearest-neighbor charge correlations with respect

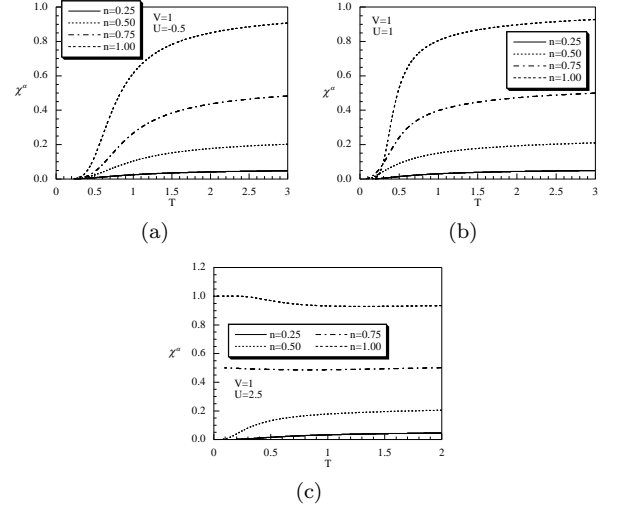


FIG. 19: The nearest-neighbor charge correlation function $\chi^\alpha = \langle n(i)n^\alpha(i) \rangle$ as a function of the temperature for different values of the particle density and (a) $U = -1/2$, (b) $U = 1$, (c) $U = 5/2$.

to higher fillings, where electrons are already clustered together.

In Fig. 20 we plot χ^α as a function of the on-site potential: one observes that χ^α is always an increasing function of U , and tends to a constant value (which depends on n), independently of the temperature, in the limit of $U \rightarrow +\infty$.

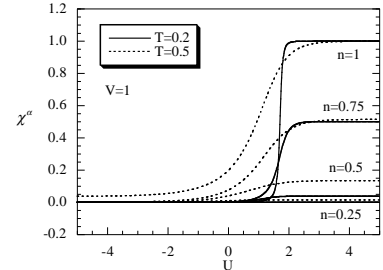


FIG. 20: The nearest-neighbor charge correlation function $\chi^\alpha = \langle n(i)n^\alpha(i) \rangle$ as a function of the on-site interaction U for $n = 0.25, 0.5, 0.75, 1$ and for $T = 0.2$ (solid lines) and $T = 0.5$ (dotted lines).

D. The compressibility

In this subsection we study the thermodynamic compressibility, defined as $\kappa = (\partial n / \partial \mu) / n^2$. In Figs. 21a-c we plot κ as a function of the filling n , for three representative values of U ($U = -V$, $U = V$ and $U = 2.1V$, respectively) and for different temperatures. To avoid divergences in the limit $n \rightarrow 0$, we plot only the derivative $(\partial n / \partial \mu)$. In the first region ($U < 0$, phase (a)), the compressibility increases by increasing n up to a maximum

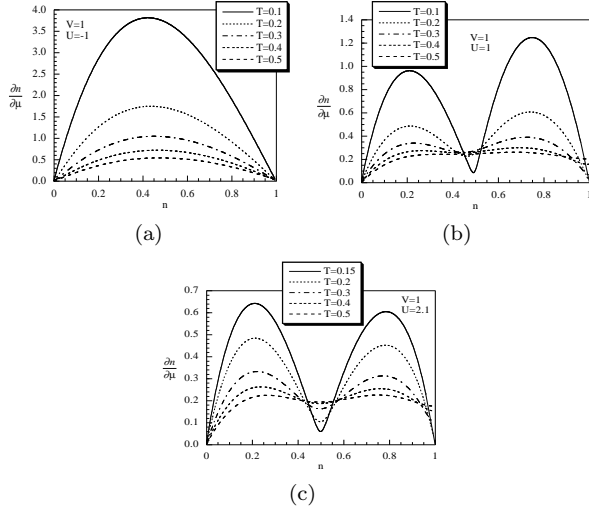


FIG. 21: $\partial n/\partial\mu$ as a function of the particle density n for various temperatures and (a) $U < 0$, (b) $0 < U < 2V$, (c) $U > 2V$.

in correspondence of quarter-filling; then it decreases exhibiting a minimum at half-filling, where a charge ordered state is established at $T = 0$ (see Fig. 3). In the second region ($0 < U < 2V$, phases (b) and (c)), κ has a double peak structure with two maxima at $n = 0.25$ and $n = 0.75$ and two minima at $n = 0.5$ and $n = 1$; the latter points correspond to the situation where a charge ordered state (checkerboard distribution for singly and doubly occupied sites, respectively) is observed at zero temperature (see Fig. 8). In the third region ($U > 2V$,

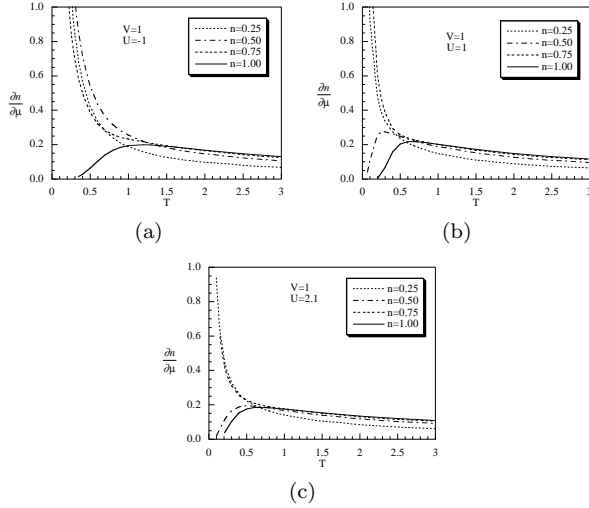


FIG. 22: $\partial n/\partial\mu$ as a function of the temperature for various fillings and (a) $U < 0$, (b) $0 < U < 2V$, (c) $U > 2V$.

phases (b) and (d)), κ has a behavior similar to the one exhibited in the second region, with the difference that the two peaks have now the same height. This difference is due to the fact that in the phase (d), for all values of

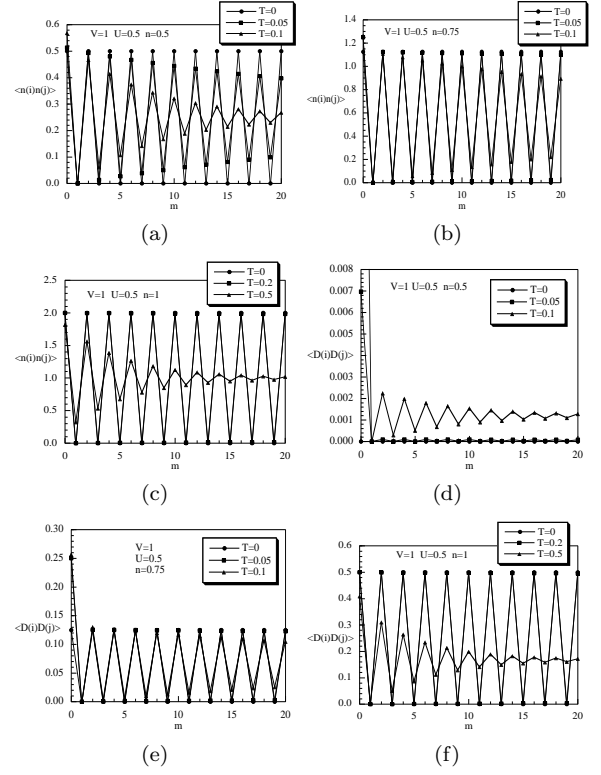


FIG. 23: The charge (a), (b), (c) and the double occupancy (d), (e), (f) correlation functions as a function of the distance $m = |i - j|$ for pertinent values of the temperature, $V = 1$ and $U = 1/2$. The value of the filling grows from left to right.

the filling, there are only singly occupied sites (see Fig. 12). In Figs. 22a-c we plot $(\partial n/\partial\mu)$ as a function of the temperature, again in the three regions of U ($U = -V$, $U = V$ and $U = 2.1V$, respectively) and for different values of the filling ($n = 0.25, 0.5, 0.75, 1$). For all values of U and n , in the limit of large temperatures, the compressibility vanishes following the law $\kappa \propto T^{-1}$, but becomes strongly filling dependent as T is reduced. In particular, in the limit $T \rightarrow 0$ and in the regions where no CO state is observed, κ increases by lowering T diverging at $T = 0$. On the other hand, in the regions where a charge ordered state is present, the compressibility exhibits a maximum at a certain temperature, then, further decreasing T , κ vanishes.

E. Correlation functions at finite temperature

At low but finite temperatures, the charge and double occupancy correlation functions $\langle n(i)n(j) \rangle$ and $\langle D(i)D(j) \rangle$ still show a finite-range order evidenced by a two-site periodicity. At quarter filling, one clearly observes in Figs. 23a and 23d that one every two sites is singly occupied: the two-site periodicity of the charge CF decreases with increasing T and distance m . The double occupancy CF is still very close to zero hinting at the ab-

sence of doubly occupied sites also at low temperatures. Upon increasing the filling, for instance at $n = 0.75$ (see Figs. 23b and 23e), both $\langle n(i)n(j) \rangle$ and $\langle D(i)D(j) \rangle$ basically retain the same zero-temperature behavior also at low temperatures. At half filling the double periodicity of the CFs persists even at higher temperatures, as evidenced in Figs. 23c and 23f.

F. Charge and spin susceptibilities

Another important quantity useful for studying the critical behavior of the system is the susceptibility. In this subsection we shall compute the charge and spin susceptibilities.

1. Charge susceptibility

Let $\Lambda(k)$ be the Fourier transform of the charge correlation function

$$\langle n(j)n(l) \rangle = \frac{a}{2\pi} \int_{-\pi/a}^{\pi/a} dk e^{ik(j-l)} \Lambda(k).$$

From Eq. (27) it is easy to derive

$$\Lambda(k) = \frac{2\pi}{a} n^2 \delta(k) + \frac{A(1-p^2)}{1+p^2-2p\cos(ka)} + \frac{B(1-q^2)}{1+q^2-2q\cos(ka)}.$$

Then, it immediately follows that the charge static susceptibility χ_c is given by

$$\chi_c = \Lambda(0) = Nn^2 + \frac{A(1+p)}{(1-p)} + \frac{B(1+q)}{(1-q)}, \quad (33)$$

where N is the number of sites. It is worthwhile to recall that χ_c can be also computed by means of the thermodynamics through the formula

$$\chi_c = Nn^2 + \frac{1}{\beta} \frac{\partial n}{\partial \mu}. \quad (34)$$

The difference between the above two expressions for χ_c lies in the fact that (33) requires the knowledge of a two-point electronic Green's function, while (34) requires only the knowledge of a one-point electronic Green's function. In condensed matter theory there are many examples where a physical quantity can be computed in different ways by using GFs of different hierarchy (see, for example, Sec. 1.5 in Ref. [59]). Of course the result should not depend on which path of calculation one has followed. This is true if one is capable to exactly solve the model. However, in many practical situations this is not possible and one needs to use some approximations. As a consequence, one may obtain different results, because approximation methods usually perform

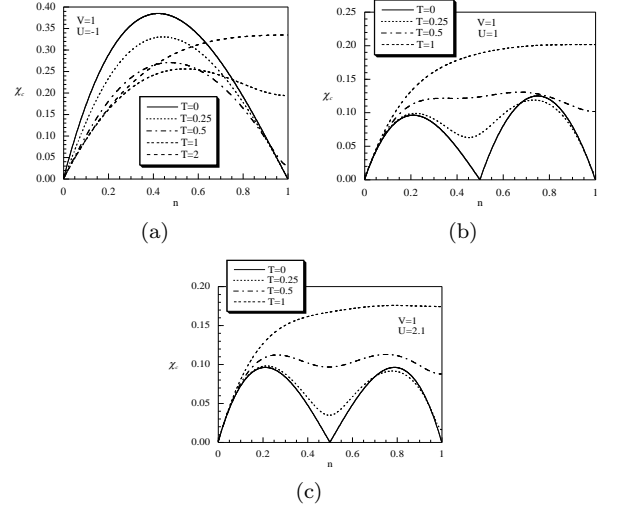


FIG. 24: The charge susceptibility as a function of the particle density for $V = 1$ and different values of the temperature, and for (a) $U = -1$; (b) $U = 1$; (c) $U = 2.1$.

in different ways according to the rank of the GFs under analysis. Actually, by comparing different expressions of the same quantity one may envisage the effectiveness of an approximation. For the present model, it is not difficult to show that Eqs. (33) and (34) give the same result since the model has been exactly solved. In the following, we will use one or the other according the convenience of numerical calculations. At $T = 0$, the charge susceptibility can be analytically computed since one knows all the coefficients A , B , p , and q , as they are given in Appendix III. In particular, one can compute χ_c in each region of the phase diagram:

$$\begin{aligned} \chi_c^{(a)} &= n(1-n)(2-n), \\ \chi_c^{(b)} &= n(1-n)(1-2n), \\ \chi_c^{(c)} &= (1-n)(2n-1), \\ \chi_c^{(d)} &= n(1-n)(2n-1). \end{aligned}$$

The superscript in the above expressions labels the different phases at $T = 0$. In Figs. 24a-c we plot χ_c as a function of the filling n for three fixed values of U ($U = -V$, $U = V$ and $U = 2.1V$, respectively) and for different temperatures. One immediately sees that, at $T = 0$, the charge susceptibility is finite except at $n = 0.5$ and $n = 1$, where, at fixed on-site potential, PTs occur. In the first region [$U < 0$, phase (a)], the charge susceptibility increases by increasing n and has a maximum in correspondence of quarter filling. Further increasing n , χ_c decreases and vanishes at half filling, where a charge ordered state is established at $T = 0$ (see Fig. 3). In the second region [$0 < U < 2V$, phases (b) and (c)], for low temperatures, χ_c has a double peak structure with two maxima around $n = 0.25$ and $n = 0.75$ and two minima around $n = 0.5$ and $n = 1$; the latter points correspond to the situation where a charge ordered state

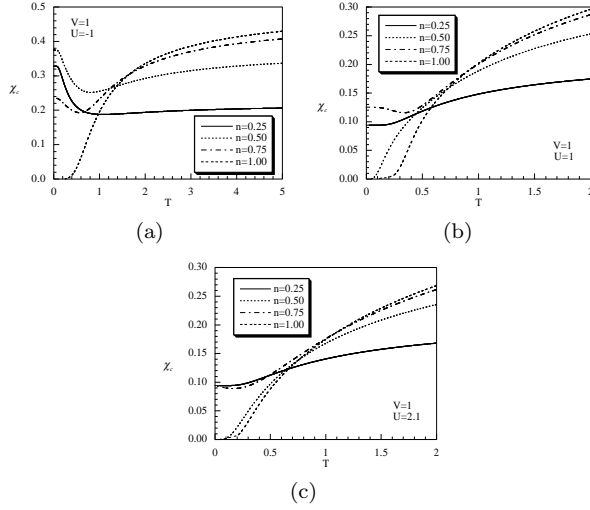


FIG. 25: The charge susceptibility as a function of the temperature for $V = 1$, $n = 0.25, 0.5, 0.75, 1$ and for (a) $U = -1$; (b) $U = 1$; (c) $U = 2.1$.

(checkerboard distribution of singly and doubly occupied sites, respectively) is observed at zero temperature (see Fig. 8). In the third region [$2V < U$, phases (b) and (d)], χ_c shows a behavior similar to the one exhibited in the second region, the difference being that the two peaks have the same height. This difference is due to the fact that in the phase (d) one has only singly occupied sites for all values of the filling (see Fig. 12). For high temperatures, χ_c is always an increasing function of n . In Figs. 25a-c we plot χ_c as a function of the temperature, again in the three regions of U ($U = -V$, $U = V$ and $U = 2.1V$, respectively) and for different values of the filling ($n = 0.25, 0.5, 0.75, 1$). For all values of U and for large temperatures, the charge susceptibility increases and tends to a constant value in the limit of T infinite. At low temperatures, one observes a different behavior: at $T = 0$, χ_c is finite for values of the particle density corresponding to nonordered states. Further increasing T , χ_c decreases, it reaches a minimum and then increases again. On the other hand, χ_c decreases with T and vanishes at $T = 0$ for fillings corresponding to charge ordered states. In the limit of high temperatures, the charge susceptibility tends to a constant value which does not depend on U but only on n according to the law

$$\lim_{T \rightarrow \infty} \chi_c = \alpha(n), \quad (35)$$

where $\alpha(n) = n(2 - n)/2$.

2. Spin susceptibility

The spin magnetic susceptibility χ_s can be computed by introducing an external magnetic field h , taking the derivative of the magnetization $m = \langle n_\uparrow(i) - n_\downarrow(i) \rangle$ with

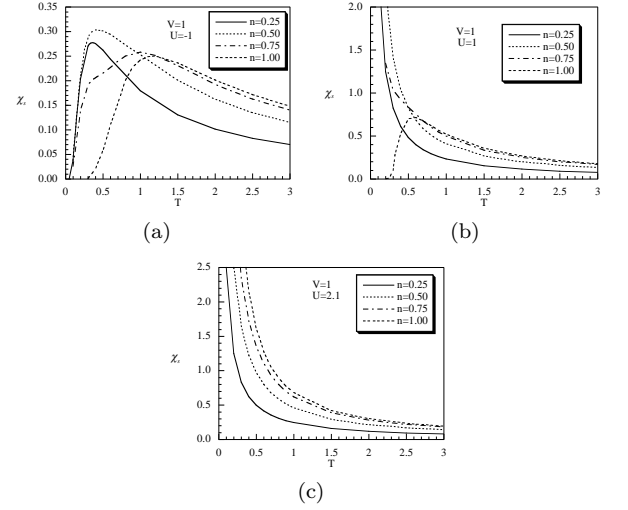


FIG. 26: The spin susceptibility as a function of the temperature for $V = 1$, $n = 0.25, 0.5, 0.75, 1$ and for (a) $U = -1$; (b) $U = 1$; (c) $U = 2.1$.

respect to h and letting h going to zero:

$$\chi_s = \left(\frac{\partial m}{\partial h} \right)_{h=0}.$$

The addition of a homogeneous magnetic field does not dramatically modify the framework of calculation given in Sec. II, once one has taken into account the breakdown of the spin rotational invariance. Details of the calculations will be presented elsewhere [61]: here we shall present only some results for the spin susceptibility χ_s relevant to our discussion. In Figs. 26a-c we plot the spin susceptibility as a function of the temperature for three representative values of U ($U = -V$, $U = V$ and $U = 2.1V$, respectively) and for different values of the filling ($n = 0.25, 0.5, 0.75, 1$). In the first region [$U < 0$, phase (a)], the spin susceptibility vanishes at zero temperature for all values of the filling: at $T = 0$ all electrons are paired and no alignment of the spin is possible. By increasing T , the thermal excitations break some of the doublons and a small magnetic field may induce a finite magnetization: χ_s augments by increasing T up to a maximum, then decreases. Calculations show that, in the limit of vanishing temperature, the behavior of χ_s in the phase (a) is

$$\lim_{T \rightarrow 0} \chi_s = \frac{n}{T} e^{-\beta(\mu - U)}.$$

The exponential behavior exhibited by the spin susceptibility is easily understood as a finite amount of energy is required to break the doublons. In the second region [$0 < U < 2V$, phases (b) and (c)], χ_s diverges at $T = 0$ for all values of the filling, but $n = 1$. At zero temperature, for $n < 1$ all the electrons singly occupy a macroscopic number of sites and their spins will align when the magnetic field is turned on. In the limit of vanishing

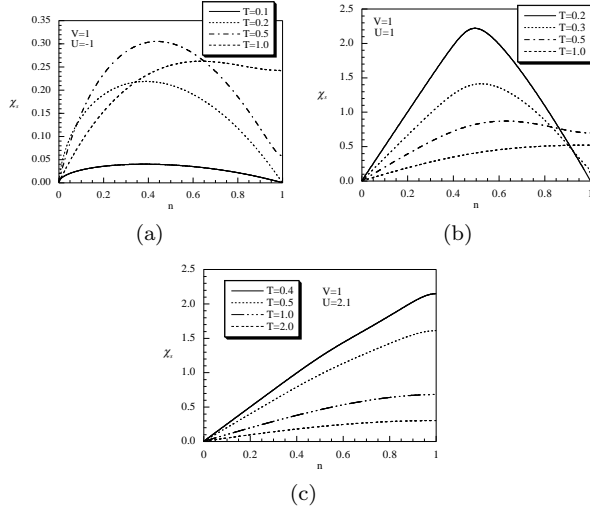


FIG. 27: The spin susceptibility as a function of the particle density for $V = 1$ and different values of the temperature, and for (a) $U = -1$; (b) $U = 1$; (c) $U = 2.1$.

temperature, χ_s diverges, according to the value of the filling, as

$$\lim_{T \rightarrow 0} \chi_s = \begin{cases} \frac{n}{T} & \text{for } 0 \leq n \leq 0.5 \quad \text{phase (b)} \\ \frac{1-n}{T} & \text{for } 0.5 \leq n < 1 \quad \text{phase (c)}. \end{cases}$$

By increasing T , the alignment is disturbed by the thermal excitations and, as a consequence, χ_s decreases. On the other hand, for $n = 1$ at $T = 0$, all electrons are paired and $\chi_s = 0$. At finite temperatures, χ_s increases linearly up to a maximum, then decreases. In the third region [$2V < U$, phases (b) and (d)] at $T = 0$ and for all values of the filling, all the sites are singly occupied: the spin susceptibility decreases with T and diverges at $T = 0$. It can be shown that in this region the spin susceptibility diverges as $T \rightarrow 0$ according to the law $\lim_{T \rightarrow 0} \chi_s = n/T$. It is easy to check that, for high temperatures, the spin susceptibility decreases with the Curie law $\chi_s \approx T^{-1}$ in the entire (U, n) plane:

$$\lim_{T \rightarrow \infty} \chi_s = \frac{\alpha(n)}{T},$$

where $\alpha(n)$ is the same U -independent function appearing in Eq. (35). As a consequence, in the limit of high temperatures, the ratio χ_c/χ_s is a universal function of T :

$$\lim_{T \rightarrow \infty} \left(\frac{\chi_c}{\chi_s} \right) = T.$$

In Figs. 27a-c we plot the spin susceptibility as a function of the particle density, again for the three representative values of U ($U = -V$, $U = V$ and $U = 2.1V$, respectively) and for different temperatures. In the first two regions χ_s has a similar behavior: it increases with n up to a maximum around $n = 0.5$, then decreases, exhibiting a minimum at $n = 1$, where at $T = 0$ all electrons are

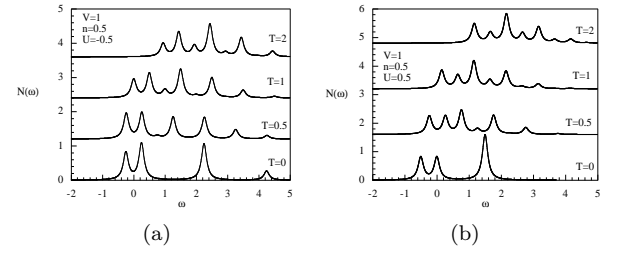


FIG. 28: The density of states $N(\omega)$ as a function of the frequency ω at quarter filling, $V = 1$, $T = 0, 0.5, 1$ and 2 for (a) $U = -1/2$; (b) $U = 1/2$.

paired. In the third region χ_s is an increasing function of n and presents a maximum at $n = 1$ where, at $T = 0$, the maximum number of singly occupied sites is present.

G. Density of states

The behavior of the density of states is, obviously, richer at finite temperatures since the thermal excitations favor the emergence of new peaks. As one can clearly see from Fig. 28, by increasing T the number of peaks increases leading to a larger number of states which the electrons can occupy. In fact, for $T \neq 0$, the weights Σ appearing in Eq. (28) are all finite. Here we report, as an example, only the DOS at quarter filling in the neighborhood of $U = 0$. One obtains similar diagrams also for other values of the filling.

H. Specific heat

The specific heat is given by

$$C = \frac{dE}{dT}, \quad (36)$$

where the internal energy E can be computed as the thermal average of the Hamiltonian (1) and it is given by

$$E = UD + 2V\lambda^{(1)}. \quad (37)$$

The specific heat exhibits a very rich structure in correspondence of the zero-temperature phase diagram shown in Fig. 1. The possible excitations of the ground state are creation and annihilation of particles in either a singly or a doubly occupied site, induced by the Hubbard operators $\psi^{(\xi)}$ and $\psi^{(\eta)}$, respectively. The corresponding transition energies are given in Eq. (7) and the peaks exhibited by the specific heat correspond to these transitions. One may distinguish between the transitions induced by $\psi^{(\xi)}$ or by $\psi^{(\eta)}$ by looking at the position of the peaks, i.e., if the position changes or remains constant by varying U . The behavior of the specific heat at $n = 0.25$ as a function of the temperature is shown in Figs. 29a-d. The specific heat presents one pronounced maximum for

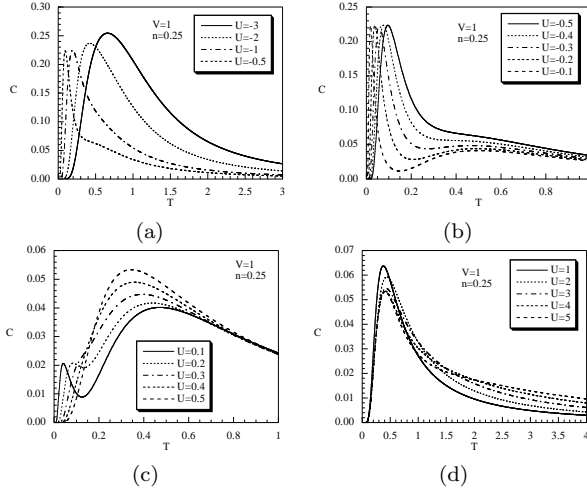


FIG. 29: The specific heat C as a function of the temperature T for $V = 1$, $n = 0.25$ and (a): $U = -3, \dots, -0.5$; (b): $U = -0.5, \dots, -0.1$; (c): $U = 0.1, \dots, 0.5$; (d): $U = 1, \dots, 5$.

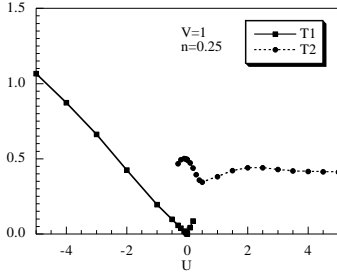


FIG. 30: The temperatures T_1 and T_2 at which the specific heat exhibits a peak are plotted as functions of U for $n = 0.25$.

large negative values of U at a temperature T_1 (see Fig. 29a). The position of the maximum decreases linearly with U until $U = 0$. Around $U \approx -0.3V$ a second peak appears at a higher temperature (see Fig. 29b). In this region, both peaks represent transitions mainly induced by $\psi^{(n)}$. The height of the first peak decreases and suddenly goes to zero at $U = 0$, where it vanishes. At $U = 0$ there is only one peak located at $T_2 \approx 0.46V$. For $U > 0$ there is a small region where the double peak structure is again present (see Fig. 29c). When $U > 0.2V$ the first peak disappears while the position of the second peak slightly increases with U up to $U \approx 2V$ where it assumes a constant value (see Fig. 29d). The behavior of T_1 and T_2 as a function of U is shown in Fig. 30. The behavior of the specific heat for this value of the filling is easily understood if one recalls that at $T = 0$, by varying U , a PT is observed at $U = 0$ from a state with doubly occupied sites to a state with singly occupied ones (see Figs. 3 and 8). Accordingly, at finite temperatures, for $U < 0$ the excitations are mainly induced by the Hubbard operator $\psi^{(n)}$ (T_1 varies linearly), while for $U > 0$ the excitations are mainly induced by $\psi^{(\xi)}$ (T_2 is constant for $U > 2V$).

In Figs. 31a-d the temperature dependence of the spe-

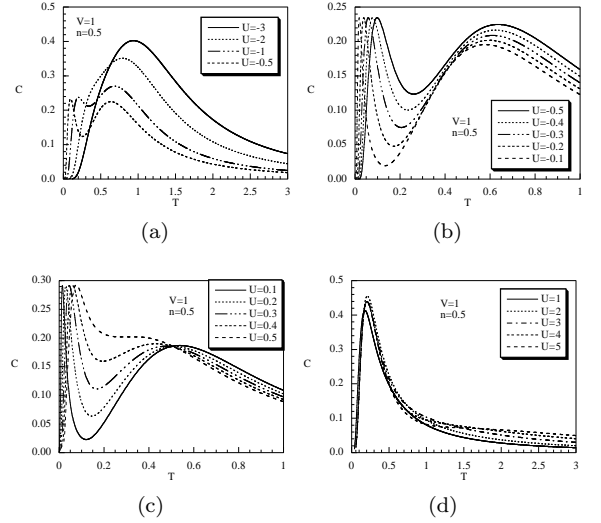


FIG. 31: The specific heat C as a function of the temperature T for $V = 1$, $n = 0.5$ and (a): $U = -3, \dots, -0.5$; (b): $U = -0.5, \dots, -0.1$; (c): $U = 0.1, \dots, 0.5$; (d): $U = 1, \dots, 5$.

cific heat is shown for $n = 0.5$. The first peak T_1 , appearing for large negative values of U (see Fig. 31a), decreases following a linear law up to $U \approx -2V$. At $U \approx -1.2V$, a second peak appears at a temperature T_2 lower than T_1 . By decreasing $|U|$, T_2 decreases linearly (see Fig. 31b). At $U = 0$ there is only one peak situated at $T_1 \approx 0.56V$. For small positive values of U , the specific heat has again two peaks (see Fig. 31c). By increasing U , T_2 increases following a linear law up to $U \approx 0.5V$; further increasing U , T_2 deviates from the linear behavior and tends to the constant value $T_2 = 0.21$ for $U > 2V$ (see Fig. 31d). The position T_1 of the first peak decreases by increasing U and, for $U > 0.5V$, the peak is no longer observable. The behavior of T_1 and T_2 as a function of U is shown in Fig. 32. It is worth noticing that, for positive U , the double peak structure is associated with the presence of a crossing point in the specific heat curves. A double peak structure, as well as the appearance of quasiuniversal crossing points, was already noticed in Refs. [10, 62] and in Sec. 3.4.2 of Ref. [59] in the Hubbard model, in Ref. [15] in an extended Hubbard-like model, and also in some experimental data [63]. When $U > V/2$ the dou-

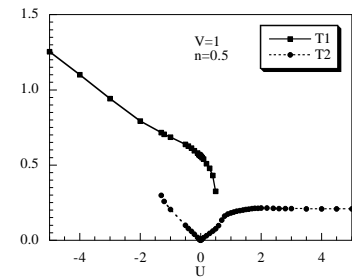


FIG. 32: The temperatures T_1 and T_2 at which the specific heat exhibits a peak are plotted as functions of U for $n = 0.5$.

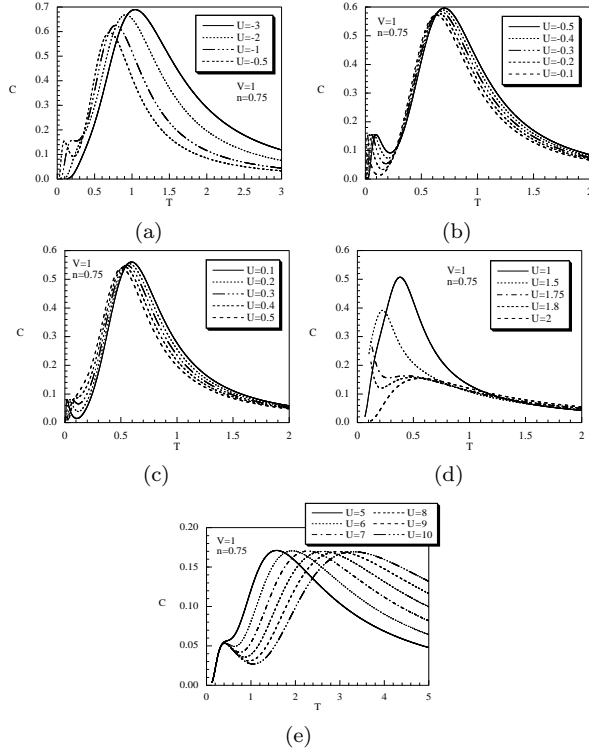


FIG. 33: The specific heat C as a function of the temperature T for $V = 1$, $n = 0.75$ and (a): $U = -3, \dots, -0.5$; (b): $U = -0.5, \dots, -0.1$; (c): $U = 0.1, \dots, 0.5$; (d): $U = 1, 1.5, 1.75, 1.8$ and 2 ; (e): $U = 5, \dots, 10$.

ble peak structure and the crossing point disappear. As for the case $n = 0.25$, the elementary excitations which mainly contribute to C for $n = 0.5$ are those induced by $\psi^{(\eta)}$ for $U < 0$ and by $\psi^{(\xi)}$ for $U > 0$.

For $n = 0.75$, as it is shown in Figs. 33a-e, one observes a double peak scenario both around $U = 0$ and $U = 2V$, in correspondence of the two different transitions observed at $T = 0$. For negative values of U , the specific heat has a peak at a temperature T_1 (see Fig. 33a) which decreases following a linear law until $U \approx 0$. Around $U \approx -V$, at a lower temperature T_2 one finds a second peak which decreases following a linear law (see Fig. 33b). At $U = 0$ there is only one peak situated at $T_1 \approx 0.62V$. For small positive values of U the specific heat has again two peaks (see Fig. 33c). By increasing U , T_2 increases following a linear law up to $U \approx 0.35V$, where this peak is no longer observable. On the other hand, the position of the first peak T_1 decreases by increasing U up to $U = 2V$, where this peak disappears. When U approaches the value $U = 2V$ a third peak appears at some temperature T_3 (see Fig. 33d). We recall that at $U = 2V$ and $T = 0$ (see Figs. 8 and 12) there is a transition from an ordered state characterized by alternating empty and occupied sites to a disordered state with only singly occupied sites. T_3 starts at $U \approx 1.75V$ and increases linearly with U . Further increasing the on-site potential one finds that at $U \approx 5.4V$ a fourth peak, situated at a lower temperature T_4 , appears (see

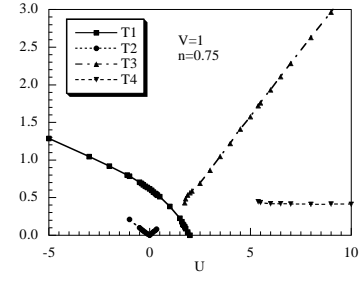


FIG. 34: The temperatures T_1 , T_2 , T_3 and T_4 at which the specific heat exhibits a peak are plotted as functions of U for $n = 0.75$.

Fig. 33e). As a result, in the region $U > 5.4V$ the specific heat exhibits a double peak structure, with T_3 increasing linearly while T_4 remains constant at the value $T_4 \approx 0.41V$. In Fig. 34 we show the behavior of T_1 , T_2 , T_3 , T_4 as functions of U . In contrast to what happens in the range $0 \leq n \leq 0.5$, for $n = 0.75$ the excitations induced by $\psi^{(\eta)}$ and by $\psi^{(\xi)}$ are both present for $U > 2V$: indeed, at $T = 0$, one observes both singly and doubly occupied sites. The behavior of the specific heat at $n = 1$ as a function of temperature is shown in Figs. 35a and 35b. When $T = 0$ and $U = 2V$, there is a PT from an ordered state with doubly occupied sites organized on a checkerboard distribution to a homogeneous state, where all the sites are singly occupied. The possible excitations are creation and annihilation of doubly occupied states. One observes a peak for negative values of U at a temperature T_1 , as shown in Fig. 36a. T_1 decreases linearly until $U \approx 0$. As U gets close to $2V$, T_1 further decreases,

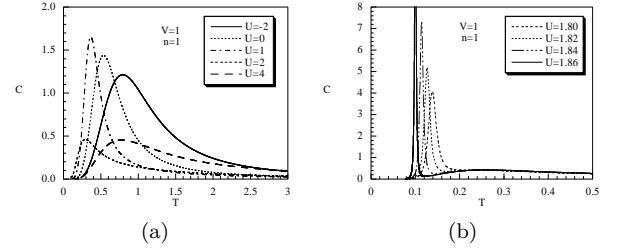


FIG. 35: (a) The specific heat C as a function of the temperature T for $V = 1$, $n = 1$ and (a) $U = -2, 0, 1, 2$, and 4 ; (b) $U = 1.8, 1.82, 1.84$ and 1.86 .

while its height h_1 exponentially increases and vanishes at $U = 2V$. T_2 appears at $U \approx 1.81V$ and increases linearly with U . When $U > 2V$, further increasing the on-site potential leads to an increase of the thermal energy required to excite an η electron above the ground state. Thus, the peak in the specific heat shifts towards higher temperatures as it is clear from Figs. 35a and 36a. In Figs. 36a-b we report the behavior of T_1 , T_2 and h_1 as a function of U . Both T_1 and T_2 vary linearly with U , according to the fact that the only possible excitations are those induced by $\psi^{(\eta)}$.

The divergence of the specific heat in the limit $U \rightarrow 2V$, when $T \rightarrow 0^+$, hints at a first order phase tran-

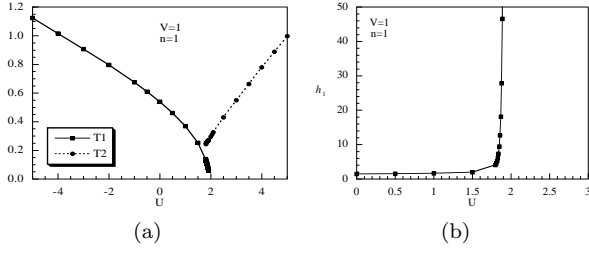


FIG. 36: (a) The temperature T_1 and T_2 as functions of the on-site potential for $V = 1$, $n = 1$. (b) The height h_1 as a function of the on-site potential for $V = 1$, $n = 1$.

sition. Another way of looking at this is to study the behavior of the internal energy. In Fig. 37 we plot the internal energy E as a function of T for several values of U just below $U = 2V$. One sees that E exhibits a jump around the related T_1 temperatures. By increasing U , the jump becomes steeper and, at the same time, smaller. In the limit $U \rightarrow 2V$, E exhibits a discontinuity with $T_1 \rightarrow 0$ and the specific heat diverges. On the other hand, at $U = 2V$, the specific heat is finite with a single peak. Sharp peaks in the specific heat at half filling, in the neighborhood of the phase transition, have also been observed in Refs. [24, 42], although with approximate methods.

To end this subsection, we want now to comment on the issue related to the two-peak structure exhibited by the specific heat. This issue has been largely discussed in the literature in the context of the ordinary Hubbard model, where the common interpretation explains the two peaks as due to spin and charge excitations. This explanation does not apply to the AL-EHM where only charge excitations are present. Our exact solution of the model points out that the possible excitations [recall the energy spectrum given in Eq. (7)] are due to a redistribution of the charge density induced by the creation and annihilation of electrons under the constraint imposed by the preexisting charge distribution. For instance, the operator $\xi^\dagger(i)n^\alpha(i)$ creates an electron at the site i , provided that this site is empty and the neighbor site(s) is (are) occupied.

Our extensive study of the U dependence of the temperature maxima T_n (at which the specific heat exhibits a peak) clearly indicates that the observed peak structure is due to charge excitations induced by the two operators $\psi^{(\xi)}$ and $\psi^{(\eta)}$. An explanation of the two peak structure, as due solely to charge excitations, has also been proposed in Ref. [15], where an exact solution of a Hubbard-like model has been given.

I. The entropy

The standard way to compute the entropy is via the derivative of the specific heat:

$$S(T) = S(0) + \int_0^T \frac{C(T')}{T'} dT'. \quad (38)$$

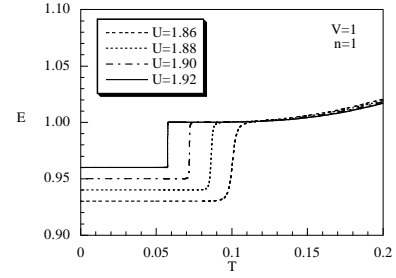


FIG. 37: The internal energy E as a function of T for $V = 1$, $n = 1$ and various values of U .

This expression requires the knowledge of the zero temperature entropy $S(0)$, which can be computed by means of the formula $S(0) = k_B \ln g$, where k_B is the Boltzmann's constant and g is the number of accessible microscopic states, i.e., all the states with energy equal to the ground state energy. Now, if the lowest energy level is non degenerate, $g = 1$ and $S(0) = 0$. On the other hand, if the lowest energy level is degenerate $g \neq 1$ and $S(0) \neq 0$. This latter situation is the one occurring in the AL-EHM: as it is shown in Figs. 3, 8, and 12, at $T = 0$, every phase (except for $n = 1$ and $U < 2V$) exhibits a macroscopic degeneracy. As a result, the zero temperature entropy is different from zero. One statement of the third law of thermodynamics is that, as the temperature approaches zero, the entropy becomes independent of the external parameters. This still holds for the AL-EHM confined in one of the possible phases. As we will show later, $S(0)$ depends on the particle density and on the on-site potential since, by varying n or U , the system can undergo a PT.

In some special cases, it is easy to compute $S(0)$. For example, from Figs. 3, 8 and 12 it is easy to see that:

(i) for $U > 0$ and $n = 0.5$, the ground state corresponds to a checkerboard distribution of singly occupied sites with arbitrary spin; the ground state energy is independent on the spin orientation and the number of accessible states is $g = (2)^{N/2}$; therefore $S(0) = \frac{N}{2} \ln(2)$.

(ii) for $U < 2V$ and $n = 1$, the ground state corresponds to a checkerboard distribution of doubly occupied sites. There is no degeneracy and, as a result, the number of accessible states is $g = 1$ and $S(0) = 0$.

(iii) for $U > 2V$ and $n = 1$, the ground state corresponds to an homogeneous distribution of singly occupied sites with arbitrary spin; the ground state energy is independent on the spin orientation and the number of accessible states is $g = (2)^N$; therefore $S(0) = N \ln(2)$.

Discarding few simple cases, it is generally not easy to compute $S(0)$. As a consequence, one has to use different formulas to compute the entropy. In the limit of infinite temperature, the entropy can be computed as $S(\infty) = k_B \ln g_\infty$, where g_∞ is the total number of states. For the model under consideration it is easy to show that

$$\lim_{T \rightarrow \infty} S(T) = 2 \log 2 - n \log(n) - (2 - n) \log(2 - n). \quad (39)$$

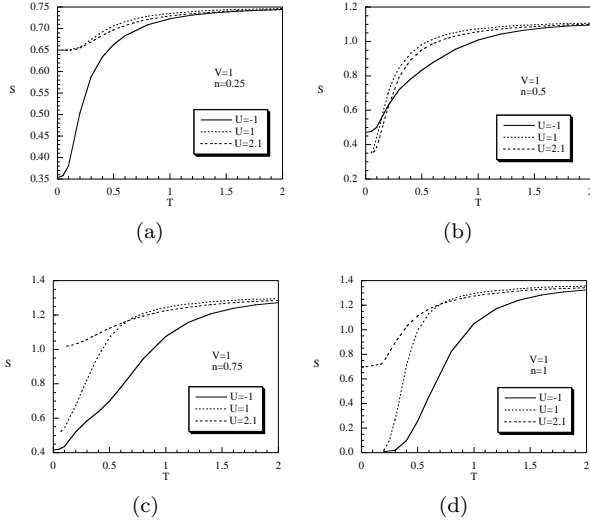


FIG. 38: The entropy S as a function of the temperature T for $V = 1$, $U = -1, 1, 2.1$ and (a): $n = 0.25$, (b): $n = 0.5$, (c): $n = 0.75$, (d): $n = 1$.

Here and in the following we set the Boltzmann's constant $k_B = 1$ and consider the entropy per site. For general values of the temperature, recalling that $(n, -\mu)$ are thermodynamically conjugated variables, one can express the entropy per site as [59]

$$S(n, T, U) = - \int_0^n \frac{\partial \mu(n', T, U)}{\partial T} dn' = \frac{1}{T} \left[E(n, T, U) - \int_0^n \mu(n', T, U) dn' \right]. \quad (40)$$

This expression requires only the knowledge of the internal energy and of the chemical potential. By making use of Eq. (40), we shall present in the following several results for the entropy as a function of T , n , and U . In Figs. 38 we plot the entropy as a function of the temperature for relevant values of the particle density n . One clearly sees that S is always a decreasing function of the temperature and that, for $n < 1$, S does not vanish for $T \rightarrow 0$. For instance, for $n = 0.75$ at $T = 0$ three phases are present by varying U : accordingly, the entropy for $T \rightarrow 0$ tends to three different constants (see Fig. 38c) which depend only on the degeneracy of the related ground state. Furthermore, it is easy to check that, in the limit $T \rightarrow \infty$, the entropy tends to the value given in Eq. (39). It is interesting to note, as it is shown in Fig. 39, that at half filling, tuning the parameter U in the neighborhood of the critical value $U = 2V$, the entropy suddenly vanishes at the same temperature T_1 at which the specific heat increases exponentially (see Fig. 35b). This can be easily understood by recalling that $C = T \cdot \partial S / \partial T$: the divergence of the specific heat is a consequence of the discontinuity of the entropy. One can think of this divergence as induced by a change from a non-degenerate state to an infinitely degenerate state.

When plotted as a function of the particle density (see

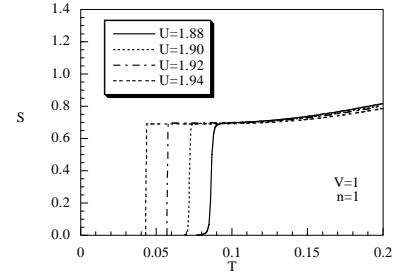


FIG. 39: The entropy as a function of the temperature for $V = 1$, $n = 1$ and different values of U close to $2V$.

Fig. 40), the entropy shows a maximum around quarter filling when one considers an attractive on-site interaction. At low temperatures, the entropy increases by increasing the particle density; it has a maximum around quarter filling and then decreases vanishing, as expected, at half filling. On the other hand, considering a repulsive on-site potential, the entropy presents a minimum at quarter filling and two maxima around $n = 0.25$ and $n = 0.75$. As evidenced in Fig. 40b, when $U > 2V$ the entropy does not vanish at half filling. The increasing and decreasing of the entropy by varying the particle density can be understood as due to the increase and decrease of the number of accessible states, as it is easy to check by looking at Figs. 3, 8, and 12. It is worthwhile to observe that the minimum values of the entropy are observed in correspondence of the ordered states, where the number of accessible states is, of course, minimum.

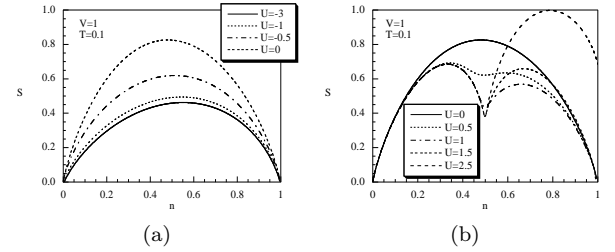


FIG. 40: The entropy S as a function of the particle density n for $V = 1$ and $T = 0.1$ (a): $U = -3, -1, -1/2$, and 0 ; (b): $U = 0, 1/2, 1, 3/2$ and $5/2$.

A useful representation of the finite-temperature phase diagram is obtained by plotting the entropy as a function of the on-site potential U , as it is shown in Figs. 41a-d. The U dependence of the entropy is rather dramatic in the neighborhood of the values at which a zero temperature transition occurs. At low temperatures, the entropy presents a steplike behavior and becomes rather insensitive to variations in U for sufficiently large on-site repulsive and attractive interactions.

When $n \leq 0.5$, the entropy presents a peak around $U = 0$ which becomes more pronounced as the temperature decreases. At quarter filling, one observes a decrease of the entropy by varying U since, in the limit $T \rightarrow 0$, the

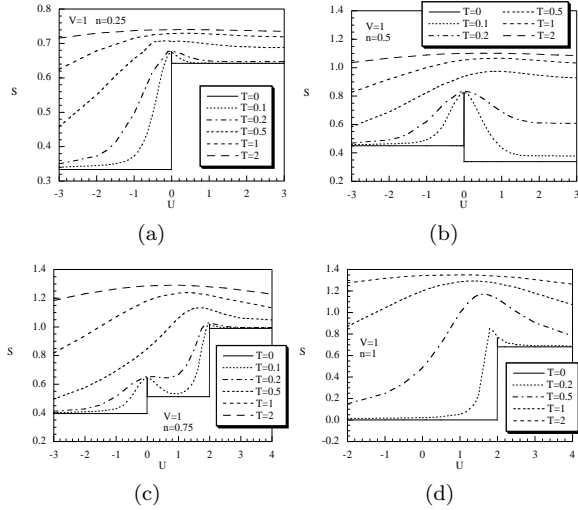


FIG. 41: The entropy S as a function of U for $V = 1$, for temperatures varying in the interval $(0, 2)$ and (a): $n = 0.25$, (b): $n = 0.5$, (c): $n = 0.75$, (d): $n = 1$.

electrons are organized in an ordered checkerboard distribution of singly occupied sites. In the region $0.5 < n < 1$, at low temperatures, one finds three regions of constant entropy corresponding to the three phases present at $T = 0$ when one moves, at fixed particle density, from negative to positive values of U . At half filling, as expected, one finds a rather sharp increase of the entropy only near $U = 2V$. In Figs. 41 we report the value $S(0)$ obtained by subtracting Eqs. (38) and (40). The study of $S(0)$ constitutes another way to detect the zero temperature transition from thermodynamic data. In fact, as it is clearly shown in Fig. 41, for each value of the electronic filling, the zero temperature entropy presents a discontinuity right at the values of the on-site potential at which one observes a phase transition.

V. CONCLUDING REMARKS

We have evidenced how the use of the Green's function and equation of motion formalism leads to the exact solution of the one-dimensional extended Hubbard model in the atomic limit. We provided a comprehensive and systematic analysis of the model by considering all the relevant correlation functions and thermodynamic quantities in the whole space of parameters n , T , and U (having chosen $V = 1$ as the unity of energy), including attractive on-site interactions. This study has shown that, at zero temperature, the model exhibits phase transitions for specific values of n and U . In particular, we have identified four phases in the (U, n) plane and PTs are observed at the borders of these phases. Various types of long-range charge ordered states have been observed: (i) at half filling and $U < 2V$, a checkerboard distribution of doubly occupied sites; (ii) at quarter filling and $U > 0$, a checkerboard distribution of arbitrary-spin singly occupied sites; (iii) in the entire region $0.5 \leq n \leq 1$ and

$0 < U < 2V$, an ordered state with alternating empty and occupied sites. The onset of a CO is signalled by the divergence of the correlation length in the charge correlation function. It is worthwhile to mention that the PT observed at half filling and $U \rightarrow 2V$ is a first order transition, as confirmed by the divergence of the specific heat and by the discontinuity in the entropy.

We derived the phase diagram by analyzing at $T = 0$ various local correlators which provide information on how the electrons are distributed on the sites of the chain. As shown in details in Secs. III and IV, the phase diagram and the observed CO states can be equivalently studied by analyzing the behavior at $T = 0$ of other quantities. The chemical potential and the double occupancy show discontinuities where PTs occur. The existence of a long-range order is well evidenced by the periodicity of the charge and double occupancy correlation functions. Another way to detect the zero temperature phase diagram is provided by the study of the behavior in the limit $T \rightarrow 0$ of the charge and spin susceptibilities and of the entropy. In particular, the entropy at zero temperature is non zero (except for $n = 1$ and $U < 2V$) and is determined only by the degeneracy of the ground state. In the limit $T \rightarrow 0$ the spin susceptibility diverges exponentially or with a power law, depending on the phase.

In Sec. IV we have studied the model at non zero temperatures. At finite but low temperatures the properties of the system are strongly determined by the zero temperature solution: a finite range order persists for a wide range of T , as evidenced by the behavior of the correlation functions. As a function of n , the charge susceptibility and the entropy exhibit a two-peak structure with minima at $n = 0.5$ and $n = 1$, where PTs are observed.

The use of equation of motion and the introduction of a closed set of composite operators $\psi^{(\xi)}$ and $\psi^{(\eta)}$, eigenoperators of H , allowed for an exact determination of the elementary excitations, $E_n^{(\xi)}$ and $E_n^{(\eta)}$, and of the relative weights $\Sigma_n^{(\xi)}$ and $\Sigma_n^{(\eta)}$. As a result, the density of states has been exactly computed for any temperature, and we performed a detailed analysis of the specific heat C . In particular, by studying the specific heat in the parameter regions corresponding to the four $T = 0$ phases, it has been possible to identify the excitations contributing to C as due to a redistribution of the charge density induced by the operators $\psi^{(\xi)}$ and $\psi^{(\eta)}$ through the creation and annihilation of electrons, provided that a charge distribution preexisted. The presence of a two-peak structure, observed in some regions of U , is explained as due to charge excitations induced by different components of the multiplet field operator $\psi^{(\eta)}$.

Acknowledgements

We thank A. Avella for stimulating discussions and a careful reading of the manuscript.

APPENDIX A: THE PARAMETERS $\kappa^{(k)}$ AND $\lambda^{(k)}$

As already mentioned in Sec. II, the use of the formalism of Green's functions and equations of motion requires two ingredients: composite operators and algebraic properties. In this Appendix we shall summarize the main results which can be obtained by exploiting the algebra satisfied by the operators. By means of the algebraic rules

$$\begin{aligned} [n(i)]^k &= n(i) + a_k D(i), \\ [D(i)]^k &= D(i), \\ [n(i)]^k D(i) &= 2^k D(i), \end{aligned} \quad (\text{A1})$$

where $a_k = 2^k - 2$ for $k \geq 1$, it is possible to derive the recursion rule

$$[n^\alpha(i)]^k = \sum_{m=1}^4 A_m^{(k)} [n^\alpha(i)]^m, \quad (\text{A2})$$

where the coefficients $A_m^{(k)}$ are rational numbers, given by

$$\begin{aligned} A_1^{(k)} &= -6 + 2^{3-k} - 2^{k-1} + 2^{3-k} \cdot 3^{k-1}, \\ A_2^{(k)} &= \frac{1}{3 \cdot 2^{k+1}} (-104 + 57 \cdot 2^{k+1} - 56 \cdot 3^k + 11 \cdot 4^k), \\ A_3^{(k)} &= \frac{1}{3 \cdot 2^{k-1}} (18 - 3 \cdot 2^{k+3} + 14 \cdot 3^k - 3 \cdot 4^k), \\ A_4^{(k)} &= \frac{1}{3 \cdot 2^{k-1}} (-4 + 3 \cdot 2^{k+1} - 4 \cdot 3^k + 4^k). \end{aligned} \quad (\text{A3})$$

It is easy to show that the relation $\sum_{m=1}^4 A_m^{(k)} = 1$ holds. As it has been shown in Sec. II C, by using the H_0 -representation, the expectation value of a generic operator O can be expressed as

$$\langle O \rangle = \frac{\langle O e^{-\beta H_I} \rangle_0}{\langle e^{-\beta H_I} \rangle_0}. \quad (\text{A4})$$

Recalling that $H_I = 2V n(i) n^\alpha(i)$ and by using the recursion rule (A2) one obtains

$$e^{-\beta H_I} = 1 + n(i) \sum_{m=1}^4 f_m [n^\alpha(i)]^m + D(i) \sum_{m=1}^4 g_m [n^\alpha(i)]^m, \quad (\text{A5})$$

where

$$\begin{aligned} f_m &= \sum_{n=1}^{\infty} (-1)^n \frac{1}{n!} A_m^{(n)} (2\beta V)^n, \\ g_m &= \sum_{n=2}^{\infty} (-1)^n \frac{1}{n!} a_n A_m^{(n)} (2\beta V)^n. \end{aligned} \quad (\text{A6})$$

By recalling Eq. (A3), one immediately sees that the coefficients f_m and g_m are polynomials of $K = e^{-\beta V}$ and

they are explicitly given by

$$\begin{aligned} f_1 &= -\frac{1}{2} K^4 + \frac{8}{3} K^3 - 6K^2 + 8K - \frac{25}{6}, \\ f_2 &= \frac{11}{6} K^4 - \frac{28}{3} K^3 + 19K^2 - \frac{52}{3} K + \frac{35}{6}, \\ f_3 &= -2K^4 + \frac{28}{3} K^3 - 16K^2 + 12K - \frac{10}{3}, \\ f_4 &= \frac{2}{3} K^4 - \frac{8}{3} K^3 + 4K^2 - \frac{8}{3} K + \frac{2}{3}, \end{aligned} \quad (\text{A7})$$

and

$$\begin{aligned} g_1 &= -\frac{1}{6} (K-1)^5 (25 + 29K + 15K^2 + 3K^3), \\ g_2 &= \frac{1}{6} (-35 + 208K - 332K^2 + 112K^3 \\ &\quad + 92K^4 - 56K^6 + 11K^8), \\ g_3 &= -\frac{2}{3} (K-1)^3 (5 - 21K - 12K^2 + 4K^3 \\ &\quad + 9K^4 + 3K^5), \\ g_4 &= \frac{2}{3} (K-1)^4 (-1 + 4K + 6K^2 + 4K^3 + K^4). \end{aligned} \quad (\text{A8})$$

One can now easily compute the parameters $\kappa^{(k)}$ and $\lambda^{(k)}$. By using Eqs. (A4) and (A5) and recalling the properties of the H_0 representation [52] one has

$$\begin{aligned} \kappa^{(k)} &= \frac{1}{\Upsilon_0} \{ \langle [n^\alpha(i)]^k \rangle_0 + \sum_{p=1}^4 (B_1 f_p + B_2 g_p) \langle [n^\alpha(i)]^{p+k} \rangle_0 \}, \\ \lambda^{(k)} &= \frac{1}{2\Upsilon_0} \{ B_1 \langle [n^\alpha(i)]^k \rangle_0 \\ &\quad + \sum_{p=1}^4 [(B_1 + 2B_2) f_p + 2B_2 g_p] \langle [n^\alpha(i)]^{p+k} \rangle_0 \}, \end{aligned} \quad (\text{A9})$$

where

$$\begin{aligned} \Upsilon_0 &= \langle e^{-\beta H_I} \rangle_0 = 1 + \sum_{p=1}^4 (B_1 f_p + B_2 g_p) [n^\alpha(i)]^p, \\ B_1 &= \langle n(i) \rangle_0 = \frac{2e^{\beta\mu}(1 + e^{\beta(\mu-U)})}{1 + 2e^{\beta\mu} + e^{\beta(2\mu-U)}}, \\ B_2 &= \langle D(i) \rangle_0 = \frac{e^{\beta(2\mu-U)}}{1 + 2e^{\beta\mu} + e^{\beta(2\mu-U)}}. \end{aligned} \quad (\text{A10})$$

By using the properties of the H_0 representation, the expectation values $\langle [n^\alpha(i)]^k \rangle_0$ can be written as

$$\begin{aligned} \langle [n^\alpha(i)]^2 \rangle_0 &= \frac{1}{2} X_1 + X_2 + \frac{1}{2} X_1^2, \\ \langle [n^\alpha(i)]^3 \rangle_0 &= \frac{1}{4} X_1 + \frac{3}{2} X_2 + \frac{3}{4} X_1^2 + \frac{3}{2} X_1 X_2, \\ \langle [n^\alpha(i)]^4 \rangle_0 &= \frac{1}{8} X_1 (1 + 7X_1) + \frac{7}{4} X_2 + \frac{9}{2} X_1 X_2 + \frac{3}{2} X_1^2, \end{aligned} \quad (\text{A11})$$

where the two parameters X_1 and X_2 are defined as

$$\begin{aligned} X_1 &= \langle n^\alpha(i) \rangle_0, \\ X_2 &= \langle D^\alpha(i) \rangle_0. \end{aligned} \quad (\text{A12})$$

Then, one has

$$\begin{aligned} \Upsilon_0 &= 1 - B_1 + B_2 + (B_1 - 2B_2)(1 + aX_1 + a^2X_2)^2 \\ &\quad + B_2(1 + dX_1 + d^2X_2)^2, \end{aligned}$$

with $a = K - 1$ $d = K^2 - 1$. The correlators $\langle [n^\alpha(i)]^k \rangle_0$ with $k > 4$ can be computed by using the recursion rule (A2). The previous formulas show that the local CFs $\kappa^{(k)}$ and $\lambda^{(k)}$ are exactly known in terms of the two basic parameters X_1 and X_2 . A similar procedure can be used for computing the other parameters $\pi^{(k)} = \langle [D^\alpha(i)]^k \rangle$, $\delta^{(k)} = \langle n(i)[D^\alpha(i)]^k \rangle / 2$, $\theta^{(k)} = \langle D(i)[D^\alpha(i)]^k \rangle / 2$. In particular, one obtains

$$\begin{aligned} \theta^{(1)} &= \frac{B_2 X_2}{2\Upsilon_0} (1 + 4a + 4b + c) [1 + (2a + b)X_1 + (c + 2b)X_2], \\ \pi^{(2)} &= \frac{1}{3}\kappa^{(4)} - \kappa^{(3)} + \frac{11}{12}\kappa^{(2)} - \frac{1}{4}n + \frac{1}{2}D, \\ \delta^{(1)} &= \frac{1}{2}\langle n(i)[D^\alpha(i)] \rangle = \frac{X_2}{2\langle e^{-\beta H_I} \rangle_0} \{ B_1(1 + 2a + b) \\ &\quad \cdot (1 + aX_1 + bX_2) + 2B_2[6a^2X_1 + b^2(4X_1 + 7X_2) \\ &\quad + c(1 + X_2 + cX_2) + a(2 + X_1 + 11bX_1 + 2cX_1 \\ &\quad + 6bX_2 + 4cX_2) + b(3 + X_1 + cX_1 + X_2 + 6cX_2)] \}, \end{aligned} \quad (\text{A13})$$

where $b = (K - 1)^2$ and $c = 4K - 4K^2 + K^4 - 1$.

APPENDIX B: NONLOCAL CORRELATION FUNCTIONS

One can define the following nonlocal correlation functions:

$$\begin{aligned} \Lambda^{(k)}(i, j) &= \langle n(i)[n^\alpha(i)]^k n(j) \rangle, \\ K^{(k)}(i, j) &= \langle [n^\alpha(i)]^k n(j) \rangle, \\ \Theta^{(k)}(i, j) &= \langle D(i)[D^\alpha(i)]^k n(j) \rangle, \\ \Pi^{(k)}(i, j) &= \langle [D^\alpha(i)]^k n(j) \rangle, \\ M^{(k)}(i, j) &= \langle D(i)[D^\alpha(i)]^k D(j) \rangle, \\ P^{(k)}(i, j) &= \langle [D^\alpha(i)]^k D(j) \rangle, \\ Q^{(k)}(i, j) &= \langle n(i)[n^\alpha(i)]^k D(j) \rangle, \\ R^{(k)}(i, j) &= \langle [n^\alpha(i)]^k D(j) \rangle, \end{aligned} \quad (\text{B1})$$

where j is a site m -steps ($m \geq 1$) distant from the site i . By using the H_0 -representation, the relevant, for our

purposes, correlation functions (B1) can be written as:

$$\begin{aligned} \Lambda^{(0)}(i, j) &= \langle n(i)n(j) \rangle = \sum_{\ell=1}^3 a_\ell Y_\ell, \\ K^{(0)}(i, j) &= \langle n(j) \rangle = \sum_{\ell=1}^3 c_\ell Y_\ell, \\ K^{(1)}(i, j) &= \langle n^\alpha(i)n(j) \rangle = \sum_{\ell=1}^3 d_\ell Y_\ell, \\ \Theta^{(0)}(i, j) &= \langle D(i)n(j) \rangle = \sum_{\ell=1}^3 b_\ell Y_\ell, \\ \Pi^{(1)}(i, j) &= \langle D^\alpha(i)n(j) \rangle = \sum_{\ell=1}^3 m_\ell Y_\ell, \\ M^{(0)}(i, j) &= \langle D(i)D(j) \rangle = \sum_{\ell=1}^3 b_\ell Z_\ell, \\ P^{(0)}(i, j) &= \langle D(j) \rangle = \sum_{\ell=1}^3 c_\ell Z_\ell, \\ P^{(1)}(i, j) &= \langle D^\alpha(i)D(j) \rangle = \sum_{\ell=1}^3 m_\ell Z_\ell, \\ Q^{(0)}(i, j) &= \langle n(i)D(j) \rangle = \sum_{\ell=1}^3 a_\ell Z_\ell, \\ R^{(1)}(i, j) &= \langle n^\alpha(i)D(j) \rangle = \sum_{\ell=1}^3 d_\ell Z_\ell, \end{aligned} \quad (\text{B2})$$

where, by assuming unitary lattice spacing, the function Y_ℓ and Z_ℓ are given by

$$\begin{aligned} Y_1 &= \langle n(j) \rangle_0, & Z_1 &= \langle D(j) \rangle_0, \\ Y_2 &= \langle n(i+1)n(j) \rangle_0, & Z_2 &= \langle n(i+1)D(j) \rangle_0, \\ Y_3 &= \langle D(i+1)n(j) \rangle_0, & Z_3 &= \langle D(i+1)D(j) \rangle_0. \end{aligned} \quad (\text{B3})$$

The coefficients a_ℓ , b_ℓ , c_ℓ , d_ℓ and m_ℓ appearing in Eqs. (B2) can be explicitly computed by means of the formulas (A4), (A10) and by using the properties of the H_0 -representation. As an example, the coefficients a_ℓ are given by:

$$\begin{aligned} a_1 &= \frac{B_1(1 + aX_1 + bX_2) + 2B_2[(a + b)X_1 + (b + c)X_2]}{\Upsilon_0}, \\ a_2 &= \frac{a^2(B_1 + 6B_2)X_1 + 2bB_2[1 + cX_2 + b(X_1 + 2X_2)]}{\Upsilon_0} \\ &\quad + \frac{a[B_1(1 + bX_2) + 2B_2(1 + 4bX_1 + 3bX_2 + 2cX_2)]}{\Upsilon_0}, \\ a_3 &= \frac{b^2(4B_2X_1 + B_1X_2 + 6B_2X_2) + 2cB_2(1 + 2aX_1 + cX_2)}{\Upsilon_0} \\ &\quad + \frac{b[B_1(1 + aX_1) + 2B_2(1 + 3aX_1 + cX_1 + 4cX_2)]}{\Upsilon_0}, \end{aligned} \quad (\text{B4})$$

where the coefficients a , b and c have been defined in Appendix A. To determine the functions Y_1 , Y_2 , Y_3 and Z_1 , Z_2 , Z_3 one requires translational invariance which leads to the following equations:

$$\begin{aligned}\langle n(i) \rangle &= \langle n(j) \rangle \Rightarrow n = \sum_{\ell=1}^3 c_\ell Y_\ell, \\ \langle D(i) \rangle &= \langle D(j) \rangle \Rightarrow D = \sum_{\ell=1}^3 c_\ell Z_\ell, \\ \langle D(i)n(j) \rangle &= \langle n(i)D(j) \rangle \Rightarrow \sum_{\ell=1}^3 b_\ell Y_\ell = \sum_{\ell=1}^3 a_\ell Z_\ell, \\ \langle D^\alpha(i)n(j) \rangle &= \langle n^\alpha(i)D(j) \rangle \Rightarrow \sum_{\ell=1}^3 m_\ell Y_\ell = \sum_{\ell=1}^3 d_\ell Z_\ell.\end{aligned}\quad (\text{B5})$$

The charge and double occupancy correlation functions can more conveniently be written in terms of the relative distance $m = |i - j|$ as

$$\begin{aligned}\Lambda^{(0)}(m) &= \langle n(i)n(i+m) \rangle = \sum_{\ell=1}^3 a_\ell Y_\ell, \\ M^{(0)}(m) &= \langle D(i)D(i+m) \rangle = \sum_{\ell=1}^3 b_\ell Z_\ell.\end{aligned}\quad (\text{B6})$$

By solving the system (B5)-(B6) one finds

$$\begin{aligned}Y_\ell &= u_\ell n + v_\ell D + w_\ell \Lambda^{(0)}(m) + z_\ell M^{(0)}(m), \\ Z_\ell &= p_\ell n + q_\ell D + r_\ell \Lambda^{(0)}(m) + s_\ell M^{(0)}(m),\end{aligned}\quad (\text{B7})$$

where the coefficients u_ℓ , v_ℓ , w_ℓ , z_ℓ and p_ℓ , q_ℓ , r_ℓ , s_ℓ are just functions of the coefficients a_ℓ , b_ℓ , c_ℓ , d_ℓ and m_ℓ . Next, we note that by definition

$$\begin{aligned}K^{(1)}(i, j) &= \frac{1}{2} \left[\Lambda^{(0)}(m+1) + \Lambda^{(0)}(m-1) \right], \\ P^{(1)}(i, j) &= \frac{1}{2} \left[M^{(0)}(m+1) + M^{(0)}(m-1) \right].\end{aligned}\quad (\text{B8})$$

Upon substituting Eqs. (B2) and (B7) in Eq. (B8) one gets

$$\begin{aligned}\Lambda^{(0)}(m+1) + \Lambda^{(0)}(m-1) &= 2 \sum_{\ell=1}^3 d_\ell \left[u_\ell n + v_\ell D + w_\ell \Lambda^{(0)}(m) + z_\ell M^{(0)}(m) \right], \\ M^{(0)}(m+1) + M^{(0)}(m-1) &= 2 \sum_{\ell=1}^3 m_\ell [p_\ell n + q_\ell D + r_\ell \Lambda^{(0)}(m) + s_\ell M^{(0)}(m)].\end{aligned}\quad (\text{B9})$$

These equations give the sought recurrence relations for the correlation function $\Lambda^{(0)}(m)$ and $M^{(0)}(m)$. As a re-

sult, one can write these equations as

$$\begin{aligned}\Lambda^{(0)}(m+1) &= W_0 \Lambda^{(0)}(m) - \Lambda^{(0)}(m-1) \\ &\quad + W_1 M^{(0)}(m) + W_2, \\ M^{(0)}(m+1) &= \Theta_0 M^{(0)}(m) - M^{(0)}(m-1) \\ &\quad + \Theta_1 \Lambda^{(0)}(m) + \Theta_2,\end{aligned}\quad (\text{B10})$$

where one has defined

$$\begin{aligned}W_0 &= 2 \sum_{\ell=1}^3 d_\ell w_\ell, & \Theta_0 &= 2 \sum_{\ell=1}^3 m_\ell s_\ell, \\ W_1 &= 2 \sum_{\ell=1}^3 d_\ell z_\ell, & \Theta_1 &= 2 \sum_{\ell=1}^3 m_\ell r_\ell, \\ W_2 &= 2 \sum_{\ell=1}^3 d_\ell [u_\ell n + v_\ell D], & \Theta_2 &= 2 \sum_{\ell=1}^3 m_\ell [p_\ell n + q_\ell D].\end{aligned}\quad (\text{B11})$$

Now, upon defining

$$\begin{aligned}G(m) &= \Lambda^{(0)}(m) - n^2, \\ F(m) &= M^{(0)}(m) - D^2,\end{aligned}\quad (\text{B12})$$

one can rewrite Eq. (B10) as

$$\begin{aligned}G(m+1) &= W_0 G(m) - G(m-1) + W_1 F(m) \\ &\quad + W_2 + W_0 n^2 - 2n^2 + W_1 D^2, \\ F(m+1) &= \Theta_0 F(m) - F(m-1) + \Theta_1 G(m) \\ &\quad + \Theta_2 + \Theta_0 D^2 - 2D^2 + \Theta_1 n^2.\end{aligned}\quad (\text{B13})$$

It is not difficult to show that the following identities do hold for any n :

$$\begin{aligned}W_2 + W_0 n^2 - 2n^2 + W_1 D^2 &= 0, \\ \Theta_2 + \Theta_0 D^2 - 2D^2 + \Theta_1 n^2 &= 0.\end{aligned}\quad (\text{B14})$$

Therefore, Eqs. (B13) simplify as

$$\begin{aligned}G(m+1) &= W_0 G(m) - G(m-1) + W_1 F(m), \\ F(m+1) &= \Theta_0 F(m) - F(m-1) + \Theta_1 G(m).\end{aligned}\quad (\text{B15})$$

The results (B14) are just a manifestation of the ergodic conditions

$$\begin{aligned}\lim_{m \rightarrow \infty} \Lambda^{(0)}(m) &= \lim_{m \rightarrow \infty} \langle n(i)n(i+m) \rangle = \langle n(i) \rangle^2, \\ \lim_{m \rightarrow \infty} M^{(0)}(m) &= \lim_{m \rightarrow \infty} \langle D(i)D(i+m) \rangle = \langle D(i) \rangle^2,\end{aligned}\quad (\text{B16})$$

which break down when there is a long range order. Examples of this scenario are shown in Sec. III. Equations (B15) together with Eq. (21) allow one to compute the correlation functions $\Lambda^{(0)}(m)$ and $M^{(0)}(m)$ for any value of m . Then, by means of Eq. (B7) one can compute the functions Y_1 , Y_2 , Y_3 , and Z_1 , Z_2 , Z_3 , whose knowledge

allows one to compute any correlation functions, by using Eq. (B2) or relative formulas. Equations (B15) show that $G(m)$ and $F(m)$ have the following form

$$\begin{aligned} G(m) &= Ap^m + Bq^m, \\ F(m) &= Cp^m + Eq^m, \end{aligned} \quad (\text{B17})$$

where the coefficients A , B , C , E , p , and q are given by

$$\begin{aligned} A &= \frac{G_0(F_2G_0 - F_0G_2) + 2G_1(F_0G_1 - F_1G_0) + G_0Q}{2Q}, \\ B &= G_0 - A, \\ C &= \frac{F_0(F_2G_0 - F_0G_2) + 2F_1(F_0G_1 - F_1G_0) + F_0Q}{2Q}, \\ E &= F_0 - C, \\ p &= \frac{F_2G_0 - F_0G_2 - Q}{2(F_1G_0 - F_0G_1)}, \\ q &= \frac{F_2G_0 - F_0G_2 + Q}{2(F_1G_0 - F_0G_1)}, \end{aligned} \quad (\text{B18})$$

with

$$\begin{aligned} Q &= [(F_2G_0 - F_0G_2)^2 \\ &\quad + 4(F_1G_0 - F_0G_1)(F_1G_2 - F_2G_1)]^{1/2}, \end{aligned} \quad (\text{B19})$$

and

$$\begin{aligned} G_0 &= G(0) = n + 2D - n^2, \\ G_1 &= G(1) = 2\lambda^{(1)} - n^2, \\ G_2 &= G(2) = 2\kappa^{(2)} - n - 2D - n^2, \end{aligned}$$

and

$$\begin{aligned} F_0 &= F(0) = D - D^2, \\ F_1 &= F(1) = 2\theta^{(1)} - D^2, \\ F_2 &= F(2) = 2\pi^{(2)} - D - D^2. \end{aligned}$$

One can rewrite Eq. (B17) as

$$\begin{aligned} G(m) &= A [\text{sign}(p)]^m e^{-m/\xi_n} + B [\text{sign}(q)]^m e^{-m/\xi_D}, \\ F(m) &= C [\text{sign}(p)]^m e^{-m/\xi_n} + E [\text{sign}(q)]^m e^{-m/\xi_D}, \end{aligned} \quad (\text{B20})$$

where the two correlation lengths ξ_n and ξ_D are defined as

$$\begin{aligned} \xi_n &= \left[\ln \left(\frac{1}{|p|} \right) \right]^{-1}, \\ \xi_D &= \left[\ln \left(\frac{1}{|q|} \right) \right]^{-1} \end{aligned} \quad (\text{B21})$$

As it has been shown in Sec. III, in the limit of zero temperature the correlation length ξ_n diverges in some regions of the (U, n) plane, signalling the presence of a phase with long-range order.

-
- [1] J. Hubbard, Proc. Roy. Soc. London, A **276**, 238 (1963).
 - [2] C. M. Varma, Sol. Stat. Comm. **62**, 681 (1987); C. M. Varma, Phys. Rev. Lett. **75**, 898 (1995); P. B. Littlewood, C. M. Varma and E. Abrahams, Phys. Rev. Lett. **63**, 2602 (1989); A. M. Janner, R. Eder, B. Koopmans, H. T. Jonkman and G. A. Sawatzky, Phys. Rev. B **52**, 17158 (1995); J. van den Brink, M. B. J. Meinders, J. Lorenzana, R. Eder and G. A. Sawatzky, Phys. Rev. Lett. **75**, 4658 (1995); J. van den Brink, R. Eder and G. A. Sawatzky, Europhys. Lett. **37**, 471 (1997).
 - [3] A. M. Gabovich, A. I. Voitenko and M. Ausloos, Phys. Rep. **367**, 583 (2002).
 - [4] E. Dagotto, *Nanoscale Phase Separation and Colossal Magnetoresistance*, Springer-Verlag, Berlin, 2002.
 - [5] J. E. Hirsch, E. Loh, Jr., D. J. Scalapino and S. Tang, Phys. Rev. B **39**, 243 (1989); P. G. J. van Dongen, Phys. Rev. Lett. **74**, 182 (1995).
 - [6] R. Pietig, R. Bulla and S. Blawid, Phys. Rev. Lett. **82**, 4046 (1999).
 - [7] A. T. Hoang and P. Thalmeier, J. Phys.: Condens. Matter **14**, 6639 (2002); N.-H. Tong, S.-Q. Shen and R. Bulla, Phys. Rev. B **70**, 085118 (2004); H. Seo, J. Merino, H. Yoshioka and M. Ogata, J. Phys. Soc. Jpn. **75**, 051009 (2006).
 - [8] D. Baeriswyl, D. K. Campbell and S. Mazumdar in *Conjugated Conducting Polymers*, edited by H. Kiess (Springer, Berlin, 1992), pp. 7134.
 - [9] M. Takahashi, Prog. Theor. Phys. **52**, 103 (1974); N. Kawakami, T. Usuki and A. Okiji, Phys. Lett. A **137**, 287 (1989); T. Usuki, N. Kawakami and A. Okiji, J. Phys. Soc. Jpn. **59**, 1357 (1990).
 - [10] A. Klümper and J. Suzuki, Nucl. Phys. B **522**, 328 (1998).
 - [11] F. Gebhard, A. Girndt and A. E. Ruckenstein, Phys. Rev. B **49**, 10926 (1994).
 - [12] H. Shiba and P. A. Pincus, Phys. Rev. B **5**, 1966 (1972); R. Schumann, Ann. Phys. (Leipzig) **11**, 49 (2001); G. W. Fernando, A. N. Kocharian, K. Palandage, Tun Wang and J. W. Davenport, Phys. Rev. B **75**, 085109 (2007).
 - [13] For a nearly exhaustive list of works studying the Hubbard model by means of numerical simulations see Ref. [59].
 - [14] A. Georges, G. Kotliar, W. Krauth and M. J. Rozenberg, Rev. Mod. Phys. **68**, 13 (1996).
 - [15] F. Dolcini and A. Montorsi, Phys. Rev. B **65**, 155105 (2002).
 - [16] D. Poilblanc, T. Ziman, J. Bellissard, F. Mila and G. Montambaux, Europhys. Lett. **22**, 537 (1993).

- [17] J. Hubbard, in *Quasi-One-Dimensional Conductors*, S. Barisic A. Bjelis, J. R. Cooper, and B. Leontic, (Springer, Berlin, 1979), Vol. 1, p. 11.
- [18] R. A. Bari, Phys. Rev. B **3**, 2662. (1971).
- [19] D. Ihle and B. Lorenz, Phys. Status Solidi B **60**, 319 (1973).
- [20] S. Robaszkiewicz, Acta Phys. Pol. A **55**, 453 (1979).
- [21] T. M. Rice and L. Sneddon, Phys. Rev. Lett. **47**, 689 (1981).
- [22] R. Micnas, S. Robaszkiewicz and K. A. Chao, Phys. Rev. B **29**, 2784 (1984).
- [23] R. S. Tu and T. A. Kaplan, Phys. Status Solidi B **63**, 659 (1974).
- [24] G. Beni and P. Pincus, Phys. Rev. B **9**, 2963 (1974).
- [25] J. Fröhlich, R. B. Israel, E. H. Lieb and B. Simon, Commun. Math. Phys. **62**, 1 (1978); J. Fröhlich, R. B. Israel, E. H. Lieb and B. Simon, J. Stat. Phys. **22**, 797 (1980).
- [26] J. Jedrzejewski, Z. Physik B **59**, 325 (1985); J. Jedrzejewski, Physica A **205**, 702 (1994).
- [27] S. A. Pirogov and Ya. G. Sinai, Theor. and Math. Phys. **25**, 1185 (1975); S. A. Pirogov and Ya. G. Sinai, *ibid.* **26**, 39 (1976); Ya. G. Sinai, *Theory of Phase Transitions: Rigorous Results*, (Pergamon Press, London 1982).
- [28] C. Borgs, J. Jedrzejewski and R. Kotecký, J. Phys. A **29**, 733 (1996).
- [29] J. Fröhlich, L. Rey-Bellet and D. Ueltschi, Commun. Math. Phys. **224**, 33 (2001).
- [30] C. Borgs and R. Kotecký, Commun. Math. Phys. **208**, 575 (2000).
- [31] H. Q. Lin, D. K. Campbell, and R. T. Clay, Chin. J. Phys. **38**, 1 (2000).
- [32] V. J. Emery, in *Highly Conducting One-Dimensional Solids*, edited by J. T. Devreese (Plenum, New York, 1979), pp. 247303; J. Solyom, Adv. in Physics **28**, 201 (1979).
- [33] M. Tsuchiizu and A. Furusaki, Phys. Rev. Lett. **88**, 056402 (2002).
- [34] B. Fourcade and G. Spronken, Phys. Rev. B **29**, 5089 (1984).
- [35] A. Luther and I. Peschel, Phys. Rev. B **9**, 2911 (1974); D. C. Mattis, J. Math. Phys. **15**, 609 (1974); J. W. Cannon and E. Fradkin, Phys. Rev. B **41**, 9435 (1990); J. Voit, Phys. Rev. B **45**, 4027 (1992).
- [36] J. E. Hirsch, Phys. Rev. Lett. **53**, 2327 (1984); J. E. Hirsch and D. J. Scalapino, Phys. Rev. B **27**, 7169 (1983); Phys. Rev. B **29**, 5554 (1984); H. Q. Lin and J. E. Hirsch, Phys. Rev. B **33**, 8155 (1986).
- [37] P. Sengupta, A. W. Sandvik and D. K. Campbell, Phys. Rev. B **65**, 155113 (2002).
- [38] J. W. Cannon, R. T. Scalettar and E. Fradkin, Phys. Rev. B **44**, 5995 (1991); C. S. Hellberg, J. Appl. Phys. **89**, 6627 (2001).
- [39] L. M. del Bosch and L. M. Falicov, Phys. Rev. B **37**, 6073 (1988); B. Fourcade and G. Spronken, Phys. Rev. B **29**, 5096 (1984).
- [40] M. Calandra, J. Merino and R. H. McKenzie, Phys. Rev. B **66**, 195102 (2002).
- [41] E. Jeckelmann, Phys. Rev. Lett. **89**, 236401 (2002); S. Ejima and S. Nishimoto, *ibid.* **99**, 216403 (2007).
- [42] S. Glocke, A. Klümper and J. Sirker, Phys. Rev. B **76**, 155121 (2007).
- [43] T. Misawa, Y. Yamaji and M. Imada, J. Phys. Soc. Jpn. **75**, 064705 (2006).
- [44] G. Pawłowski, Eur. Phys. J. B **53**, 471 (2006).
- [45] M. Aichhorn, H. G. Evertz, W. von der Linden and M. Potthoff, Phys. Rev. B **70**, 235107 (2004).
- [46] M. Nakamura, J. Phys. Soc. Jpn. **68**, 3123 (1999); Phys. Rev. B **61**, 16377 (2000).
- [47] K. M. Tam, S. W. Tsai and D. K. Campbell, Phys. Rev. Lett. **96**, 036408 (2006).
- [48] K. Sano and Y. Ōno, Phys. Rev. B **75**, 113103 (2007).
- [49] F. Mila and X. Zotos, Europhys. Lett. **24**, 133 (1993); K. Penc and F. Mila, Phys. Rev. B **49**, 9670 (1994).
- [50] W. P. Su and J. R. Schrieffer, Phys. Rev. Lett. **46**, 738 (1981).
- [51] S. Mazumdar, H. Q. Lin and D. K. Campbell, in *Organic Superconductivity*, edited by V. Z. Kresin and W. A. Little (Plenum, New York, 1990), pp. 221229.
- [52] F. Mancini, Eur. Phys. J. B **47** 527, (2005).
- [53] F. Mancini, Europhys. Lett. **70**, 484 (2005); Condens. Matter Phys. **9**, 393 (2006).
- [54] F. Mancini, Euro Phys. Journ. B **45**, 497 (2005).
- [55] A. Avella and F. Mancini, Eur. Phys. J. B **50**, 527 (2006).
- [56] F. Mancini and A. Naddeo, Phys. Rev. E **74**, 061108 (2006).
- [57] L. Onsager, Phys. Rev. **65**, 117 (1944).
- [58] F. Mancini, F. P. Mancini and A. Naddeo, J. Opt. Adv. Mat. **10**, 1688 (2008).
- [59] F. Mancini and A. Avella, Adv. Phys. **53**, 537 (2004).
- [60] F. Mancini, S. Marra and H. Matsumoto, Physica C **250**, 184 (1995).
- [61] F. Mancini and F. P. Mancini, preprint:unisa/cond-mat/002072008, submitted.
- [62] D. Duffy and A. Moreo, Phys. Rev. B **55**, 12 918 (1997).
- [63] A. Germann and H. V. Löhneysen, Europhys. Lett. **9**, 367 (1989); G. E. Brodale, R. A. Fisher, N. E. Phillips, and J. Flouquet, Phys. Rev. Lett. **56**, 390 (1986); F. Steglich C. Geibel, K. Gloos, G. Olesch, C. Schant, C. Wassilew, A. Loidl, A. Krimmel, and G. R. Stewart, J. Low Temp. Phys. **95**, 3 (1994).